Sheet on a deformable sphere: Wrinkle patterns suppress curvature-induced delamination

Evan Hohlfeld and Benny Davidovitch
Department of Physics, University of Massachusetts, Amherst, Massachusetts 01003, USA
(Received 1 August 2013; revised manuscript received 18 November 2014; published 20 January 2015)

The adhesion of a stiff film onto a curved substrate often generates elastic stresses in the film that eventually give rise to its delamination. Here we predict that delamination of very thin films can be dramatically suppressed through tiny, smooth deformations of the substrate, dubbed here "wrinklogami," that barely affect the macro-scale topography. This "prolamination" effect reflects a surprising capability of smooth wrinkles to suppress compression in elastic films even when spherical or other doubly curved topography is imposed, in a similar fashion to origami folds that enable construction of curved structures from an unstretchable paper. We show that the emergence of a wrinklogami pattern signals a nontrivial isometry of the sheet to its planar, undeformed state, in the doubly asymptotic limit of small thickness and weak tensile load exerted by the adhesive substrate. We explain how such an "asymptotic isometry" concept broadens the standard usage of isometries for describing the response of elastic sheets to geometric constraints and mechanical loads.

DOI: 10.1103/PhysRevE.91.012407 PACS number(s): 68.35.Np, 46.32.+x

I. INTRODUCTION

A. Background

The adhesion of stiff films onto curved topographies is required for common operations, such as placing bandages on knuckles or noses, and underlies a broad range of technologies, from producing a hemispherical electronic eye [1] to wear-resisting coating of joint implants [2]. When the adhesive film is sufficiently large the elastic stress required to maintain its attachment to the curved substrate increases the energetic cost of adhesion, and the film delaminates. Despite its obvious importance, studies of such a geometry-induced delamination, and more broadly, of the basic mechanisms by which a curved shape can be imposed on a solid film whose stress-free state is planar, appeared only recently. These studies have focused on the deformations of solid films and their consequent delamination from curved substrates that are effectively infinitely rigid [3–5]. Here and in a subsequent paper [6], we seek to provide a general theoretical framework to this fundamental problem. Our purpose is to characterize the various morphological types exhibited by an adhesive film on a curved substrate that is either rigid or deformable and the relevant dimensionless groups of parameters that govern the laminated state of the film and its ultimate delamination from the substrate. For simplicity, and to discuss the problem in a context that is close to some recent experiments, we choose to focus our work on the behavior of thin films attached to a spherically shaped substrate.

Considering a spherical substrate, one may notice that delamination of an adhesive film has a similar origin to the unavoidable distortion of distances in planar maps of Earth. Assuming, for instance, a direct projection of a circular film of radius W on a large rigid sphere of radius $R \gg W$, one may estimate the average strain in the film as $(W/R)^2$, the approximate percentage by which longitudes are elongated [see Fig. 1(a)]. The elastic energy cost (per area) is $U \sim (E_f t)(W/R)^4$, where E_f is the Young's modulus and t the thickness of the film, and delamination occurs when this energy exceeds the areal adhesion energy density Γ [7]. Noting that the fraction ϕ of the sphere covered by the film is proportional to $(W/R)^2$, we obtain the maximal laminated fraction of a rigid sphere [3]:

$$\phi_{\rm rig} \sim \sqrt{\Gamma/E_f t}. \tag{1}$$

This scaling law has been confirmed in recent experiments that used a glass ball as a substrate [4]. However, in another experiment, in which the rigid substrate was replaced with a liquid drop, delamination was not observed even when the coverage fraction ϕ was apparently much larger than $\phi_{\rm rig}$ [8]. Instead, the radial profile of the drop was gradually flattened beneath the attached film, deviating substantially from the original spherical shape of the drop [Fig. 1(c)]. Furthermore, the drop-film system developed a periodic pattern of radial wrinkles of tiny wavelength and amplitude, indicating the relaxation of compression along latitudes near the perimeter of the film [Fig. 1(b)].

The observations of a distinctive behavior of adhesive films on rigid and liquid substrates motivates our theoretical study of adhesion on a deformable, curved solid substrate. The simplest model system that enables us to study this problem is the adhesion of a thin elastic film on a spherically shaped Winkler foundation of radius R and stiffness K, which may be thought of as a ball of N harmonic springs, each with rest length R and spring constant $4\pi R^2 K/N$ [Fig. 1(d)]. The simplified nature of the Winkler's response allows us to carry out a quantitative analysis, from which we extract the scaling laws that govern the adhesion and delamination of a thin solid film on real, isotropic, spherically shaped solid substrate, of radius R and Young's modulus E_s.

B. Main results

1. Prolamination

A central prediction of our study is that, in addition to the two aforementioned classes of adhesion on rigid and soft substrates, there exists a novel type of adhesion where the film delaminates at a coverage fraction $\phi_{\rm def} \gg \phi_{\rm rig}$ without any macro-scale deformation of the spherically shaped substrate. We call this delamination suppression phenomenon *"prolamination"* and argue that as the film becomes thinner it is expected to prevail at a broad range of physical parameters, denoted below as "regime III." For an isotropic, spherically

 ©2015 American Physical Society

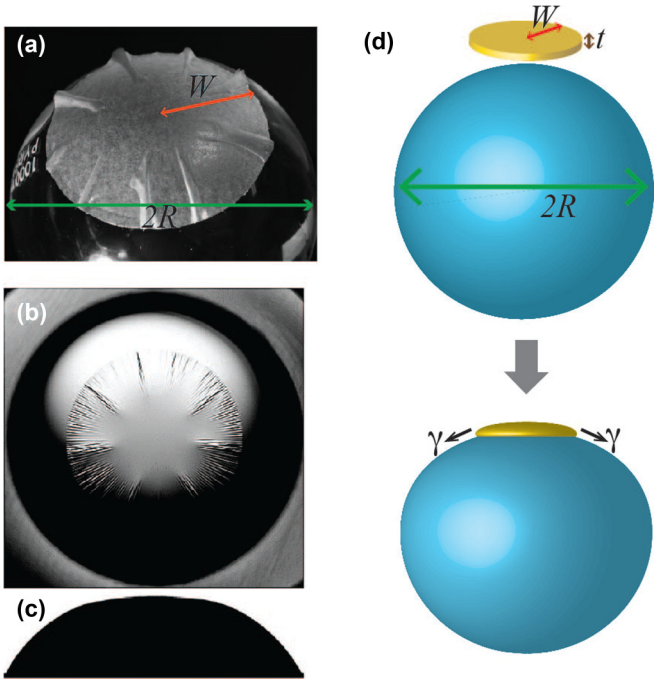

FIG. 1. (Color online) (a) A thin adhesive film delaminates from a glass ball of radius R when its area ($\sim W^2$) exceeds a critical fraction $\phi_{\rm rig}$ [Eq. (1)] of the surface area of the ball ($\sim R^2$). Before delamination, longitudes of the film acquire an average strain $\sim(W/R)^2$. (b),(c) Top and side views of an ultrathin PS film floating on a curved liquid surface (see [8]). The film remains attached to the surface, and the joint deformation consists of flattening of the liquid portion beneath the film (c) and a periodic array of radial wrinkles (b). Courtesy of H. King and N. Menon. (d) Schematic figure of our model system: a thin disk (yellow, light gray) of Young's modulus E_f, thickness t, and radius W is attached to a spherical substrate (blue, dark gray) of radius $R \gg W$, by the substrate-vapor surface tension γ that pulls on the film's edge. (For simplicity, we assume $\gamma \approx \Gamma$, where Γ is the adhesion energy; see Sec. II B 2.) The resistance of the substrate to deformation of its spherical shape is modeled through a Winkler's stiffness K (a ball of N springs, each with an effective constant $4\pi R^2 K/N$). The generalization to the case of an isotropic solid with Young's modulus E_s is discussed in Sec. V B.

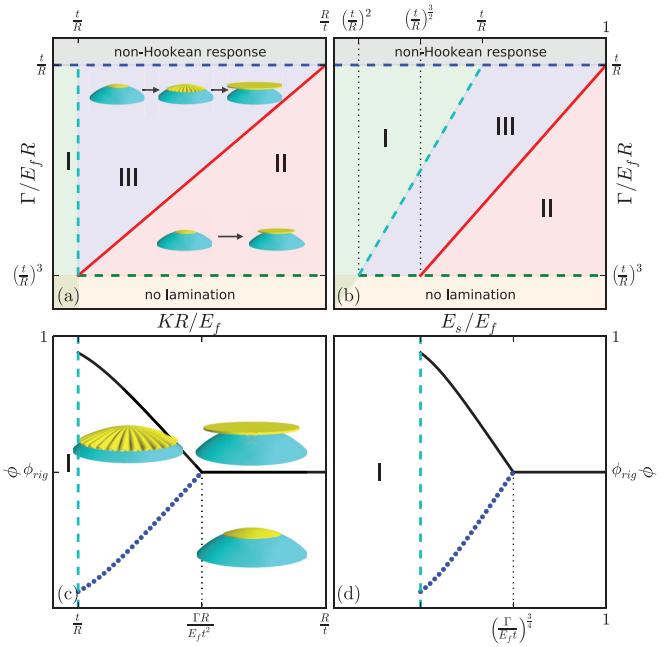

FIG. 2. (Color online) (a) Phase diagram for the adhesion of thin films on curved substrates. Regime I (green, light gray): Soft substrates are deformed significantly, suppressing elastic strain and thus delamination at all values of the coverage fraction ϕ. Regime II (red, medium gray): Rigid substrates are undeformed, and the film is severely strained. For a given point in regime II we illustrate the delamination process upon increasing ϕ. Regime III (blue, dark gray): For substrates with intermediate stiffness, both their macro-scale deformation and strain in the laminated film are suppressed by forming fine wrinkles for $\phi_{\rm wr} < \phi < \phi_{\rm def}$. Delamination occurs at $\phi = \phi_{\rm def} \gg \phi_{\rm rig}$ [Eqs. (54b) and (56b)]. In the "no lamination" regime (amber, below lower horizontal dashed line), the energetic cost of bending precludes any adhesion. The boundaries between regimes II/III and III/I are described, respectively, by the relations: $K_{\rm rig} \sim \Gamma/t^2$ [Eq. (51)] and $K_{\rm soft} \sim (E_f t)/R^2$ [Eq. (52)]. Logarithmic scales are used for the axes, making the phase boundaries appear as straight lines. (b) An analogous phase diagram for an elastic substrate with modulus E_s. The lines that separate regimes II/III and III/I, are, respectively, $E_{s,\rm rig} \sim \gamma^{3/4} E_f^{1/4}/t^{3/4}$ [Eq. (57)] and $E_{s,\rm soft} \sim \gamma^{1/2} E_f^{1/2} t^{1/2}/R$ [Eq. (61)]. (c) Varying the substrate stiffness K, we plot the predicted evolution of the system for a fixed adhesion energy Γ and film's thickness t as the coverage fraction ϕ increases. The blue (dotted) curve is described by Eqs. (54a) and (56a), and the black (solid) curve is described by Eqs. (54b) and (56b). Delamination occurs above the black (solid) curve, wrinkling occurs between the blue (dotted) curve and black (solid) curve, and large substrate deformations occur to the left of the cyan (vertical dashed) line. (d) An analogous diagram to (c) for an elastic substrate with modulus E_s.

shaped solid substrate, this prediction is borne out by identifying two distinct characteristic values of the substrate's Young's modulus, $E_s^{\rm soft}$ and $E_s^{\rm rig}$, which mark the transitions between three different regimes of adhesion. The explicit dependence of $E_s^{\rm soft}$ and $E_s^{\rm rig}$ on the physical parameters (film's thickness and modulus, substrate radius, and strength of adhesion) is described in Fig. 2(b) [see also Eqs. (57) and (61)].

Regime I: $E_s < E_s^{\rm soft}$, where delamination is totally suppressed and the substrate is substantially deformed beneath the film, similarly to a liquid drop.

Regime II: $E_s > E_s^{\rm rig}$, where the substrate is effectively rigid and delamination occurs at $\phi = \phi_{\rm rig}$ [Eq. (1)].

Regime III: $E_s^{\rm soft} < E_s < E_s^{\rm rig}$. In this intermediate regime, the film delaminates from the substrate at a coverage fraction $\phi_{\rm def}$, which may significantly exceed $\phi_{\rm rig}$ if the film is sufficiently thin [see Fig. 2(d)].

The *prolamination* effect in parameter regime III is enabled by wrinkles around the original shape of the substrate, whose amplitude decreases with the film's thickness t. In contrast to adhesion on a liquid drop (or regime I above), the substrate retains its spherical shape and does not deform beneath the film, except for those tiny wrinkles. Notably, we find that the ratio $E_s^{\rm soft}/E_s^{\rm rig}$ becomes indefinitely small as the film's thickness diminishes, so that regime III is prominent for the adhesion of ultrathin films. For instance, for a polystyrene film ($E_f \approx 3$ GPa) of thickness $t = 100$ nm attached to spherical substrate of radius $R = 1$ cm with adhesion energy $\Gamma = 70$ dyn/cm, we find that the system is within the intermediate

regime III if the sphere is made of material similar in stiffness to polydimethylsiloxane ($E_s \approx 2$ MPa). For a graphene sheet (estimating $E_f \approx 1$ TPa and $t \approx 0.1$ nm [9] and assuming similar values of R and Γ), where wrinkling and delamination are often observed [10], we find that this parameter regime is obtained for substrates whose stiffness can be as large as a few GPa (e.g., low- and high-density polyethylene).

How does the wrinkle pattern suppress delamination of the film? As we explained above, curvature-induced delamination stems from the strain, $\sim(W/R)^2$, acquired by a flat film of size W upon placing it on a sphere of radius R. The energetic cost of strain is proportional to the stretching modulus $\sim E_f t$. Recalling the Gauss' *theorema egregium*, which links the strain (i.e., deviation from a flat metric of a manifold) to the Gaussian curvature, it is tempting to think that such a geometry-induced strain in the film is inevitable, and so is the elastic energy cost associated with it. However, we find that the wrinkle pattern acts precisely to diminish almost entirely this strain, such that the energetic cost becomes governed by the bending modulus of the film, $B \sim E_f t^3$, and the deformation energy of the substrate. For a sufficiently thin film, this reduction in the energetic cost makes the laminated state more favorable in comparison to the loss of adhesion due to delamination. This reduction in the energetic cost, and the fact that it requires merely tiny perturbation of the substrate rather than macro-scale deformation of its shape, underlies the prolamination effect.

2. Asymptotic isometry and the "wrinklogami" pattern

Beyond its importance for the adhesion of films, the wrinkle pattern that enables the prolamination effect constitutes a novel type of *asymptotic isometry* of elastic films. The common usage of "isometry" in elasticity theory refers to a perfectly strainless mapping of a surface (the film's midplane) to some configuration in three-dimensional (3D) space. This familiar mathematical concept is particularly useful for describing the "stress focusing" of thin solid sheets under geometric confinement (e.g., sheet confined by a ring [11,12] or a box [13]), whereby the shape attains a piecewise-developable shape, namely, a state which is strainless everywhere except in narrow ridges and vertices that become lines and points as the sheet's thickness $t \to 0$ [11,12,14–16]. The "asymptotic isometry equation" that we introduce in this paper (Sec. VI B) generalizes this concept, showing that a film may approach an isometry even when its boundary is subjected to a weak tensile load, rather than to a purely geometric confinement. This asymptotic isometry equation characterizes the energy of a family of states, parametrized by two parameters—the film's thickness t and the tension γ exerted on the film's edge—that approach an isometry in the limit $(t \to 0, \gamma \to 0)$.

In addition to highlighting the relevance of isometric maps to sheets subjected to geometric confinement and weak tensile loads, our analysis broadens the type of physically admissible states through which the strain can be eliminated, showing that such states are not necessarily (piecewise) developable, stress-focusing patterns. Instead, we show that asymptotically isometric states could be associated with wrinkle patterns that emanate from a nearly homogenous collapse of both compressive and tensile parts of the stress throughout the film. We think that such a homogenous, simultaneous collapse of both compressive and tensile stress is rather surprising and deserves its own label, since the common emergence of wrinkle patterns is associated with the collapse of compression only, whereas the tensile stress along the wrinkle direction is retained. We propose the word wrinklogami (which is different though from "buckligami" [17]) to highlight the conceptual similarity to origami artistry that creates curved structures from unstretchable sheets through designed networks of sharp (inelastic) folds [18,19].

C. Outline

We start in Sec. II with a detailed description of the physical constants, the energies, and the various forces in our model system; those pertain to the elastic film, the deformable substrate, and the adhesion between them. We conclude this section by listing the dimensionless groups of parameters that govern the problem: the geometrical and mechanical strains, their ratio (called confinement), the bendability, and the deformability parameter. In Sec. III we discuss the unwrinkled, axisymmetric state of the system, where a reduction of the strain in the laminated film is associated with large deformation (flattening) of the substrate. This discussion highlights the physical meaning of the deformability parameter and enables us to identify a range of parameters where the laminated state is only slightly deformed from a spherical shape. This parameter range includes regimes II and III in Fig. 2 and is the main focus of the rest of the current paper. In Sec. IV we analyze the effect of the wrinkle pattern on the laminated state of a film attached to such a slightly deformable spherical substrate. We start by explaining the "far-from-threshold" approach, used in recent studies of radially stretched sheets, and employ it to evaluate the energy gain due to the formation of wrinkles. In contrast to previous studies, the focus of our analysis here is on the parameter regime of large confinement and large bendability, corresponding to the limit $(t \to 0, \gamma \to 0)$ at which the wrinkle pattern becomes an asymptotic isometry of the laminated film. In Sec. V we construct the phase diagrams in Figs. 2(a) and 2(b), by comparing the energies of the unwrinkled and wrinkled states with the energy cost of delamination. We start with the Winkler substrate of stiffness K, assumed throughout our study, and then "translate" the relevant scaling laws to an isotropic elastic substrate with Young's modulus E_s. Finally, in Sec. VI we discuss the concept of asymptotic isometry, its applicability for other systems, and the framework it provides for studying morphological transitions between wrinkles and deformation patterns that are governed by stress focusing.

In a subsequent paper [6] we plan to elaborate on the physics in parameter regime I in Fig. 2, which corresponds to an adhesive film on a curved, highly deformable substrate.

II. MODEL

The laminated state in our model system consists of surface energy U_{sur}, as well as the energies U_{Win}, U_{strain}, and U_{bend}, which are associated, respectively, with the deformation of the spherical substrate (modeled by Winkler's response) and the straining and bending of the laminated film. These energies are expressed as functionals of the displacement field, and the associated strain and curvature of the film. We start this section by describing these fields.

A. Displacement, strain, stress, and normal force

We consider a circular elastic film of radius W attached to a spherical substrate of radius R, as depicted in Fig. 1(d). For our current study it is sufficient to address the case $W \ll R$; hence, we use the common theory, often attributed to Föppl and von Kármán (FvK), which assumes the amplitude and slope of the deformed film are small everywhere. (Our theory can be developed with the aid of covariant derivatives in the full geometrically nonlinear framework, but this complication is not required in the current study). Additionally, we assume that the strains are small, which allows us to use a Hookean stress-strain relation (namely, linear material response). In this simplified framework the two tangential directions can be taken to be the radial $\hat{\boldsymbol{r}}$ and azimuthal $\hat{\boldsymbol{\theta}}$ at the plane of the undeformed film and the normal direction $\hat{\boldsymbol{n}}$ to be along the perpendicular $\hat{\mathbf{z}}$ to that plane. The displacement field is then expressed as

$$\mathbf{u}(r,\theta) = \mathrm{u}_r(r,\theta)\hat{\mathbf{r}} + \mathrm{u}_\theta(r,\theta)\hat{\boldsymbol{\theta}} + \zeta(r,\theta)\hat{\mathbf{z}}. \tag{2}$$

1. Strain and stress

The strain tensor $\boldsymbol{\varepsilon}$ is given by

$$\varepsilon_{rr} = \partial_r \mathrm{u}_r + \frac{1}{2}(\partial_r \zeta)^2, \tag{3a}$$

$$\varepsilon_{\theta\theta} = \frac{1}{r}\partial_\theta \mathrm{u}_\theta + \frac{1}{r}\mathrm{u}_r + \frac{1}{2r^2}(\partial_\theta \zeta)^2, \tag{3b}$$

$$\varepsilon_{r\theta} = \varepsilon_{\theta r} = \frac{1}{2}\left(\frac{1}{r}\partial_\theta \mathrm{u}_r + \partial_r \mathrm{u}_\theta + \frac{1}{r}\partial_r \zeta \partial_\theta \zeta\right), \tag{3c}$$

and the stress in the film is given by the Hookean relationship [20–22]

$$\sigma_{rr} = \frac{Y}{1-\Lambda^2}\left(\varepsilon_{rr} + \Lambda\varepsilon_{\theta\theta}\right), \tag{4a}$$

$$\sigma_{\theta\theta} = \frac{Y}{1-\Lambda^2}\left(\varepsilon_{\theta\theta} + \Lambda\varepsilon_{rr}\right), \tag{4b}$$

$$\sigma_{r\theta} = \frac{Y}{1+\Lambda}\varepsilon_{r\theta}, \tag{4c}$$

where $Y = E_f t$ is the stretching modulus and Λ the Poisson ratio of the sheet [23].

2. Curvature

Since we assume the shape $\zeta(r,\theta)$ to be characterized by small slopes, the various components of the curvature tensor κ_{ij} can be approximated as

$$\kappa_{rr} = \partial^2_{rr}\zeta, \quad \kappa_{\theta\theta} = \frac{1}{r}\partial_r\zeta + \frac{1}{r^2}\partial^2_{\theta\theta}\zeta, \quad \kappa_{r\theta} = \left(\partial_r - \frac{1}{r}\right)\partial_\theta\zeta. \tag{5}$$

3. Winkler's restoring force

As we mentioned already, the simplest model for a curved solid substrate is a Winkler's sphere of radius R and stiffness K, which exerts a restoring force $F_{\mathrm{Win}}(\mathbf{x}) = -K[r(\mathbf{x}) - R]$ for deviations of its spherical shape (where $\mathbf{x}$ is a point on the surface of the substrate and $r(\mathbf{x})$ is the distance of this point from the center of the spherical substrate). Since $W \ll R$, the Winkler's restoring force on the film and the attached substrate can be approximated as

$$\mathbf{F}_{\mathrm{Win}}(r,\theta) \approx -K[\zeta(r,\theta) - r^2/2R]\hat{\mathbf{z}}. \tag{6}$$

The Winkler model is advantageous, both conceptually and computationally, due to the local nature of the substrate response [24]. We assume a fixed K throughout the analysis, and explain in Sec. V how the results can be used to describe the behavior of an elastic substrate with Young's modulus E_s by identifying an appropriate "effective stiffness."

B. Energies

Here we discuss the energy of the system and the boundary conditions implied on deformations of the laminated film at its perimeter, $r = W$, by the surrounding surface of the substrate. We denote actual energies as $\bar{U}_{(\cdot)}$, energy densities (per area) as $U_{(\cdot)} = \bar{U}_{(\cdot)}/W^2$, and the normalized (dimensionless) energies as $u_{(\cdot)}$, where

$$u_{(\cdot)} \equiv \bar{U}_{(\cdot)}/(E_f t)W^2 \tag{7}$$

(and similarly for work terms, which are denoted by the normal typeface W and w). Note that the normal typeface u stands for the displacement field, whereas the italic u stands for energy normalized by $(E_f t)W^2$. For clarity, we derive first the actual energies, $\bar{U}_{(\cdot)}$, and only later introduce their normalized versions, $u_{(\cdot)}$.

1. Adhesion energy

Before discussing the energetic cost of an elastic film laminated on a spherical substrate, let us consider two "ideal" configurations: a delaminated state, where the film is completely detached from the substrate (except, perhaps, at a few isolated points or lines), and an unstretchable film (i.e., with $E_f = \infty$) attached to a planar substrate. It is useful to define the adhesion energy $\bar{U}_{\mathrm{ad}}$ as the energetic difference between these two ideal states,

$$\bar{U}_{\mathrm{ad}} = \Gamma A \equiv (\gamma_{\mathrm{fil,vap}} - \gamma_{\mathrm{fil,subst}} + \gamma)A, \tag{8}$$

where $A = \pi W^2$ is the area of the film, $\gamma_{\mathrm{fil,vap}}$, $\gamma_{\mathrm{fil,subst}}$, are the surface tensions (energies per molecular area) of the film-vapor and film-substrate interfaces, respectively, and γ is the surface tension of the substrate-vapor interface.

Two notes are in order here. First, the actual energy of the laminated state consists of additional contributions, due to the strain and curvature of the film, which are the subject of the subsequent subsections. Second, it is possible that as delamination occurs, the film retains partial contact with the substrate, as is shown in Fig. 1(a). Nevertheless, as long as some finite portion of the film detaches from the substrate, the energetic cost of delamination can be estimated through Eq. (8) multiplied by an appropriate numerical prefactor.

2. Work of adhesive substrate on elastic film

Equation (8) defines the energy $\bar{U}_{\mathrm{ad}}$ by considering the laminated state of an unstretchable film on a planar substrate, where the area of the film is $A = \pi W^2$. When studying a solid film with finite stretching modulus Y attached to a spherical substrate of radius R, we must consider also the induced changes in surface area, which give rise to additional contributions to surface energy: $(\gamma_{\mathrm{fil,subst}} + \gamma_{\mathrm{fil,vap}})\, dA_{\mathrm{fil}}$ and $-\gamma\, dA_{\mathrm{sph}}$. Here dA_{fil} is the modification to the area of the deformed film, and dA_{sph} is the modification to the area

removed from the substrate-vapor surface due to the laminated film. The explicit expressions for $dA_{\rm fil}$ and $dA_{\rm sph}$ are

$$dA_{\rm film} = \int dS\, \varepsilon_{ii}, \tag{9a}$$

$$dA_{\rm sph} = 2\pi W[{\rm u}_r(W) + W^3/8R^2], \tag{9b}$$

where in Eq. (9a) ε_{ii} is the trace of the strain tensor [Eq. (3)] and the integral is over the range $r < W$. In Eq. (9b), we obtained the term $W^3/8R^2$ by considering the radial displacement ${\rm u}_r(W)$ of the film's edge for an area-preserving, axisymmetric projection of the film onto a rigid sphere [25]. Note that, generally, $dA_{\rm film} \neq dA_{\rm sph}$; namely, the total surface area (of substrate-vapor, substrate-film, and film-vapor) is not necessarily conserved. An equality ($dA_{\rm fil} = dA_{\rm sph}$), which for a planar substrate is trivially satisfied, would have been achieved only if the film was axisymmetrically stretched on the sphere, such that the radial displacement at its edge is ${\rm u}_r(W) = -W^3/8R^2$ [25].

A central outcome of the forthcoming analysis is the strong deviation of the laminated film from the highly energetic axisymmetric state, which is enabled by the formation of wrinkles such that $|dA_{\rm sph}/dA_{\rm fil}| \gg 1$. The physical meaning of this result is that the laminated film can remain almost unstretched ($dA_{\rm fil} \approx 0$) by forming a larger substrate-vapor contact area, such that $dA_{\rm sph} < 0$. Therefore, we find that the surface energy of the laminated state can be approximated through the expression

$$\bar{\rm W}_{\rm surf} = -\gamma\, dA_{\rm sph} = -2\pi\gamma W[{\rm u}_r(W) + W^3/8R^2], \tag{10}$$

which is simply the tensile work exerted by the adhesive spherical substrate on the edge of the laminated film.

Since the tangential force exerted on the perimeter of the film, $r = W$, is simply the derivative of this work with respect to the radial displacement of the edge ${\rm u}_r(W)$, we obtain the boundary condition:

$$\sigma_{rr}(W) = \gamma. \tag{11}$$

Since the three surface tensions $\gamma_{\rm fil,subst}$, $\gamma_{\rm fil,vap}$, and γ are separate physical constants, the adhesion energy Γ [Eq. (8)] and the tensile boundary force [Eq. (11)], are two independent quantities. For simplicity, we assume in the current study $\gamma \approx \Gamma$, but our results (up to numerical factors that do not affect the scaling rules) are valid for any finite ratio of γ/Γ.

3. Substrate deformation

The energy associated with the local, Winkler-type restoring force, Eq. (6), is

$$\bar{U}_{\rm Win} = \tfrac{K}{2} \int d^2x\, [r(\mathbf{x}) - R]^2, \tag{12}$$

where the integration is over the whole surface area of the substrate. This energy, which penalizes for deviations from the favorable spherical shape of the substrate, can be written as

$$\bar{U}_{\rm Win} = \tfrac{K}{2} \int_0^{2\pi} d\theta \int_0^W r dr\, (\zeta - r^2/2R)^2 + \bar{U}_{\rm men}, \tag{13}$$

where the integral is now only over the substrate surface beneath the laminated film and, similarly to Eq. (6), we used $W/R \ll 1$ to express the leading order (in W/R) of this term. The second term $\bar{U}_{\rm men}$ in Eq. (13) corresponds to the "meniscus," deformation of the substrate's surface that decays away from the film's edge at $r = W$. In Appendix A we show that any effects of the energy $\bar{U}_{\rm men}$ can be safely neglected in our analysis.

4. Bending energy

The bending energy of the curved film is proportional to the square of the principal curvatures. For $W/R \ll 1$ and with our polar coordinates this energy becomes

$$\bar{U}_{\rm bend} = \frac{B}{2} \int_0^{2\pi} d\theta \int_0^W r dr[(\partial_{rr}\zeta)^2 + (r^{-2}\partial_{\theta\theta}\zeta)^2 + 2r^{-2}\partial_{rr}\zeta\,\partial_{\theta\theta}\zeta], \tag{14}$$

where $B = Et^3/[12(1-\Lambda^2)]$ is the bending modulus of the film. The minimal bending energy for a film of area $\sim W^2$ on a substrate with curvature R^{-1} is $\bar{U}_{\rm bend} \sim (B/2)W^2/R^2$, implying that the adhesion Γ must exceed a critical value $B/R^2 \sim E_f t^3/R^2$ in order for the film to be laminated. This lower bound underlies the horizontal dashed green line in the phase diagram [Figs. 2(a) and 2(b)]. In this study we address the parameter regime $\Gamma \gg E_f t^3/R^2$ (or $\delta_m \gg \tilde{t}^2$ in the dimensionless parameters, to be defined below), where the bending cost associated with the substrate curvature R^{-1} can be neglected [26].

If the film is sufficiently thin (and the substrate is not too rigid) the wrinkle pattern governs the bending energy due to the high curvature of the small wavelength undulations in the azimuthal direction. Hence, Eq. (14) can be approximated by

$$\bar{U}_{\rm bend} = \frac{B}{2} \int_0^{2\pi} d\theta \int_0^W r\, dr\, (r^{-2}\partial_{\theta\theta}\zeta)^2. \tag{15}$$

5. Straining energy

Imposing a spherical shape on the film will generally give rise to elastic stresses σ_{ij} in the plane of the film (where $i,j = r,\theta$) and to corresponding strains ε_{ij} [Eq. (4)]. The energy associated with these stresses is

$$\bar{U}_{\rm strain} = \frac{1}{2} \int_0^{2\pi} d\theta \int_0^W r\, dr \sigma_{ij}\varepsilon_{ij}. \tag{16}$$

C. The Föppl-von Kármán equations

At mechanical equilibrium, the system can be described by the FvK equations of elastic sheets,

$$B\Delta^2\zeta - \sigma_{rr}\partial_r^2\zeta - \frac{2}{r}\sigma_{r\theta}\left(\partial_r - \frac{1}{r}\right)\partial_\theta\zeta - \frac{1}{r^2}\sigma_{\theta\theta}\left(\partial_\theta^2\zeta + r\partial_r\zeta\right) = -K[\zeta(r,\theta) - r^2/2R], \tag{17a}$$

$$\partial_r\sigma_{rr} + \frac{1}{r}(\partial_\theta\sigma_{r\theta} + \sigma_{rr} - \sigma_{\theta\theta}) = 0, \tag{17b}$$

$$\partial_r\sigma_{r\theta} + \frac{1}{r}(\partial_\theta\sigma_{\theta\theta} + 2\sigma_{r\theta}) = 0, \tag{17c}$$

where the Laplacian $\Delta \equiv \partial_r^2 + \frac{1}{r}\partial_r + \frac{1}{r^2}\partial_\theta^2$ and the stress-strain relations [Eqs. (4)] with the geometric strain-displacement relation [Eqs. (3)] are used to transform Eqs. (17) to a nonlinear set of partial differential equations for the three

components of the displacement field $\mathbf{u}(r,\theta)$. Equation (17a) is the first FvK equation and expresses force balance in the normal direction; Eqs. (17b) and (17c) form the second FvK equation and express force balance on each infinitesimal piece of the film in the two directions locally tangent to the sheet [20–22]. These equations can be obtained as the Euler-Lagrange equations of the energy functional $\bar{U}_{\rm strain} + \bar{U}_{\rm bend} + \bar{U}_{\rm Win}$.

At the parameter regime that we focus on here, which is relevant for very thin films, the bending energy due to radial curvature and the force associated with it $[=B(\partial_r^2 + \frac{1}{r}\partial_r)^2\zeta]$ are always negligible.

In the following sections we show that this fact allows us to analyze the FvK equations (17) both for the axisymmetric (unwrinkled) state and for the fully wrinkled state of the system, by using the boundary conditions (BCs) at $r = W$,

$$\sigma_{rr}(W) = \gamma, \tag{18a}$$

$$\zeta(W) = \zeta_{\rm sph}(W), \quad \frac{\partial}{\partial r}\zeta(W,\theta) = \zeta'_{\rm sph}(W), \tag{18b}$$

where $\zeta_{\rm sph}(r) \approx -r^2/2R$ is the shape of the undeformed sphere. The BC (18a) follows from Eq. (11), and the second BC (18b) stems from the negligibility of normal force and torque exerted on the film's edge by the deformed substrate at $r > W$. In Appendix A we explain why BC (18b) is valid for a slightly deformable substrate, which is the main focus of our study, as well as for a highly deformable substrate, which we plan to discuss elsewhere.

Two other BCs at $r = 0$ are

$$\mathrm{u}_r(0) = 0, \quad \zeta_r(0) = 0, \tag{19}$$

which imply integrity of the film and a nondiverging stress at its center.

D. Dimensionless groups

1. From dimensional parameters to dimensionless groups

The physical (dimensional) parameters of our model are the substrate-vapor surface tension (γ), the adhesion energy per area (Γ), the stiffness (K), and radius (R) of the substrate and the Young's modulus (E_f), thickness (t), and radius (W) of the film. All energies considered, denoted hence by lowercase $u_{(\cdot)}$, are normalized by the stretching modulus ($E_f t$) and the area W^2 of the film, such that the model can be characterized by five dimensionless groups:

$$\delta_g = (W/R)^2, \quad \delta_m = \gamma/(E_f t), \quad \tilde{t} = t/R, \tag{20}$$

$$\tilde{K}^{-1} = (E_f t)/K R^2, \tag{21}$$

$$\gamma/\Gamma \approx 1. \tag{22}$$

We call the first two numbers, respectively, the *geometrical* and *mechanical* strains (δ_g,δ_m) that are imposed on the film and elaborate on their physical meaning in the next paragraph. The number $\tilde{t}$ is a useful dimensionless measure of the sheet's thickness, which simplifies the appearance of various formulas. The fourth dimensionless group, $\tilde{K}^{-1}$, which we call the *deformability* parameter, is the only one that depends on the substrate stiffness K [27]. In the following section we highlight the basic difference between a high deformability regime ($\tilde{K}^{-1} \gg 1$) and the low-deformability regime ($\tilde{K}^{-1} \ll 1$), on which we focus in this paper. Finally, the ratio between the substrate-vapor surface tension and the adhesion energy is another independent dimensionless group, but in the current study we assume for simplicity that it is identically one [28].

The division of the four primary dimensionless groups in Eqs. (20) and (21) reflects an important feature of our model. Although δ_g, δ_m, and $\tilde{t}$ are independent parameters, we show below that the morphology of the laminated state depends only the deformability $\tilde{K}^{-1}$ and two independent combinations of the triplet (δ_g,δ_m,$\tilde{t}$), which we call the effective *confinement* and *bendability* parameters. In order to understand their meaning, let us discuss first the strain parameters.

2. Geometrical strain, mechanical strain, and confinement

The mechanical strain δ_m is defined as the tensile strain at the film's perimeter $r = W$, which exists also in the lamination of a flat substrate. Such a tensile load tends to induce uniform tension $\sim\gamma$, and hence expansion of both longitudes and latitudes across the film. In contrast, the geometrical strain δ_g imposed on the film is associated with the projection of a flat shape onto a sphere and therefore induces confinement of latitudes. This basic difference between the imposed geometrical strain and mechanical strain is a cornerstone of our study. We show that, in contrast to the mechanical strain, the geometrical strain does not necessarily imply stretching or compressing the film; instead, the film may "trade in" such a highly energetic straining with wrinkles whose energetic cost is associated with bending the sheet and deforming the substrate. This difference underlies the asymptotic isometry that may be attained by the film and the prolamination phenomenon. In order to elucidate the conflicting nature of the geometrical and mechanical strains it is useful to introduce their ratio,

$$\alpha = \delta_g/\delta_m = (E_f t)W^2/\gamma R^2, \tag{23}$$

which was called the *confinement* parameter in [8,29]. The parameter α describes the degree of confinement of latitudes imposed on the film by stretching it over a spherical substrate.

As we mentioned in the beginning of this section, it is sufficient for us to consider small values of both geometrical and mechanical strains, δ_g,$\delta_m \ll 1$, such that the coverage fraction ϕ of the sphere laminated by the film satisfies $\phi \sim (W/R)^2 \sim \delta_g \ll 1$, and the stress is proportional to the strain, as we discussed in Secs. II A and II C. The condition $\delta_m \ll 1$ underlies the upper bound in the phase diagram, Fig. 1(a): If $\Gamma > (E_f t)$, the adhesion is too strong and the large strain may generate non-Hookean response. (The lower boundary in Fig. 1(a) is explained in Sec. II B 4 and in [26].)

3. The bendability parameter

In addition to the deformability parameter $\tilde{K}^{-1}$ and the confinement α, another crucial ratio for understanding the system is the effective *bendability*, denoted as ϵ^{-1}, which expresses the ratio between the imposed strain and the bending resistance of the film. This ratio is conveniently expressed as the product of the von Kármán number $\nu K = (W/t)^2$, which characterizes the aspect ratio of the film, and the characteristic

TABLE I. "Pristine" dimensionless groups of the model.

Group	Definition	Focus of current study	Comments
Normalized thickness	$\tilde{t} = t/R$	$\tilde{t} \ll \phi^2$	Compression collapses by wrinkling (Sec. IV A)
Mechanical strain	$\delta_m = \gamma/E_f t$	$\tilde{t}^2 \ll \delta_m \ll 1$	Hookean response (Sec. II B 1) Adhesion sufficiently strong (Sec. II B 4)
Geometric strain	$\delta_g = (W/R)^2$	$\delta_g \sim \phi \ll 1$	Small slopes, FvK equations are valid (Sec. II C)
Laminated fraction of sphere	$\phi \sim \delta_g$		
Deformability	$\tilde{K}^{-1} = (E_f t)/(K R^2)$ [27]	$\tilde{K}^{-1} \ll 1$	Low substrate deformability (Sec. III B)
Tensile ratio	γ/Γ	≈ 1	Simplification (Sec. II D)

imposed strain $= \max[\delta_g, \delta_m]$:

$$\epsilon^{-1} \sim vK \times (\text{imposed strain}) \begin{cases} = \epsilon_m^{-1} = \frac{\gamma W^2}{B} & (\alpha < 1), \\ = \epsilon_g^{-1} = \frac{W^4}{t^2 R^2} & (\alpha > 1), \end{cases} \tag{24}$$

where we refer to ϵ_m^{-1} and ϵ_g^{-1}, respectively, as the *mechanical and geometrical bendabilities*, in analogous manner to the mechanical and geometrical strains, δ_m and δ_g, introduced above. Note that the definition (24) of the bendability parameter generalizes previous usage of this term [8,29–33] which addressed only the "mechanical regime," where $\epsilon = \epsilon_m$.

4. *Three relevant dimensionless groups and asymptotic limits*

Recent works on radially stretched elastic films described the characteristic morphologies in these systems through two dimensionless parameters: confinement and bendability. The study of an elastic film laminated on a solid substrate requires us to consider three dimensionless groups: the generalized versions of the confinement and bendability parameters, Eqs. (23) and (24), and the substrate deformability $\tilde{K}^{-1}$ [Eq. (21)].

In terms of the effective confinement, bendability, and deformability parameters, the core of the current paper is analysis of the parameter regime $\tilde{K}^{-1} \ll 1$, $\alpha \gg 1$, $\epsilon^{-1} \gg 1$. The assumption of low deformability ($\tilde{K}^{-1} \ll 1$) allows us to simplify calculations since the shape of the laminated shape is close to the original, spherical shape of the substrate. This assumption, which is used intensively in the next sections, will be relaxed in a subsequent paper [6], where we plan to address also the high-deformability regime. The focus on high confinement and bendability values is the essential contribution of the present work. The asymptotic limit $\alpha \to \infty$, which in dimensional form reads $\gamma \ll (E_f t)(W/R)^2$, means that the mechanical strain is negligible in comparison to the geometric strain; the asymptotic limit $\epsilon\,(=\epsilon_g) \to 0$, which in dimensional form reads $t \ll W^2/R$, means that the imposed geometric strain can be eliminated by wrinkles. Thus, when the tension imposed on the film is weak enough and the film's thickness is sufficiently small, we have to study the doubly asymptotic limit $(\alpha, \epsilon^{-1}) \to \infty$ at a fixed value of $\tilde{K}$. This singular limit, on which we expand further in Sec. IV D, underlies the concept of asymptotic isometry that we study here.

An additional complexity stems from the nontrivial dependence of those effective parameters on the four "pristine" dimensionless parameters, Eqs. (20) and (21). Therefore, Fig. 1(a) (or any other planar plot of the phase diagram) must be understood as a projection of this 4D parameter space onto a specific planar section. In Tables I and II we summarize the dimensionless parameters of our model and specify the parameter regimes that are the focus of the current study.

III. THE AXISYMMETRIC STATE

We start with the laminated, axisymmetric state of the system, whose energy underlies the delamination from a highly rigid substrate [Eq. (1)] [3,5]. The analysis, which is focused on the high bendability limit, will allow us to elucidate the role of the geometric and mechanical strains, δ_g and δ_m, the confinement parameter α, and the deformability parameter $\tilde{K}^{-1}$.

The axisymmetric state is characterized by radial and normal displacements of the form $\mathrm{u}_r(r), \zeta(r)$. The only components of the strain tensor are

$$\varepsilon_{rr} = \mathrm{u}_r' + \tfrac{1}{2}(\zeta')^2, \quad \varepsilon_{\theta\theta} = \mathrm{u}_r/r, \tag{25}$$

and the corresponding components of the stress tensor are $\sigma_{rr}(r), \sigma_{\theta\theta}(r)$, as determined from Eq. (4). The FvK equations (17) thus transform into a coupled set of ordinary differential equations (ODEs) for the functions $\mathrm{u}_r(r), \zeta(r)$,

$$\partial_r \sigma_{rr} + \frac{1}{r}(\sigma_{rr} - \sigma_{\theta\theta}) = 0, \tag{26a}$$

$$\sigma_{rr}\partial_r^2 \zeta + \frac{1}{r}\sigma_{\theta\theta}(\partial_r \zeta) = K[\zeta - r^2/2R], \tag{26b}$$

where we neglected the bending force due to the radial curvature R^{-1} (see Sec. II B 4). These equations, together with Eqs. (4) and (25), are second order in u_r and ζ, and therefore the BCs (18) and (19) suffice to find the axisymmetric state. Notably, solutions to these FvK equations are determined by two dimensionless groups only: the confinement parameter $\alpha = \delta_g/\delta_m$ and the deformability parameter $\tilde{K}^{-1}$. We denote these solutions by the superscript axi; for instance, the stress components are denoted as $\sigma_{rr}^{\mathrm{axi}}(r; \tilde{K}, \alpha)$, $\sigma_{\theta\theta}^{\mathrm{axi}}(r; \tilde{K}, \alpha)$. We address first the case of an infinitely rigid substrate and then turn to discuss deformable substrates.

A. Strain and confinement

An infinitely rigid, undeformable substrate must keep its spherical shape; hence, $\zeta(r) = \zeta_{\mathrm{sph}} \approx -r^2/2R$. In this case, Eqs. (26) can be solved analytically [3] and we find

$$\sigma_{\theta\theta}^{\mathrm{axi}}(r; \tilde{K} = \infty, \alpha) = \gamma\{\alpha[1 - 3(r/W)^2]/16 + 1\},$$
$$\sigma_{rr}^{\mathrm{axi}}(r; \tilde{K} = \infty, \alpha) = \gamma\{\alpha[1 - (r/W)^2]/16 + 1\}. \tag{27}$$

TABLE II. Effective dimensionless parameters.

Group	Definition	Focus of current study	Physical meaning
Confinement	$\alpha = \delta_g/\delta_m$	$\alpha \gg 1$	Asymptotic isometry (Sec. IV A)
Mechanical bendability	$\epsilon_m^{-1} = \tilde{t}^{-2}\delta_m\delta_g$		
Geometrical bendability	$\epsilon_g^{-1} = \tilde{t}^{-2}\delta_g^2$	$\epsilon_g^{-1} \gg \epsilon_m^{-1} \gg 1$	Asymptotic isometry (Secs. IV A)
Deformability	$\tilde{K}^{-1}$ (see above)	$\tilde{K}^{-1} \ll 1$	Low substrate deformability

Thus, up to a constant factor (γ), the stresses are completely determined by the confinement parameter $\alpha = \delta_g/\delta_m$. Obviously, for a substrate of infinite stiffness, the substrate deformation energy vanishes, and the energy of the axisymmetrically laminated film is dominated by the part $\bar{U}_{\rm strain}$ [Eq. (16)], whose normalized version $\bar{U}_{\rm strain}/(E_f t)W^2$ becomes

$$u^{\rm axi} = \pi\delta_m^2\left[-1+\Lambda+\tfrac{1}{384}\alpha^2\right]. \tag{28}$$

These exact expressions for the stress and energy provide us an insight into the nature of the axisymmetric state, which is useful also for the case of a deformable substrate. When the confinement α is small, the tension exerted by the substrate on the film is sufficiently strong (alternatively, curvature is sufficiently weak), and both stress components are tensile everywhere. In this range, the normalized elastic energy can be estimated as $u^{\rm axi} \sim \delta_m^2$, independent of the coverage fraction ϕ. In contrast, when $\alpha \gg 1$, the strong geometric strain induces azimuthal compression ($\sigma_{\theta\theta} < 0$) near the perimeter, at a zone that extends as α increases. At large confinement ($\alpha \gg 1$) the energy of the axisymmetric state becomes dominated by the geometric strain $u^{\rm axi} \sim \delta_g^2 \sim \phi^2$. We thus obtain the asymptotic scaling rules:

$$u^{\rm axi}(\phi) \sim \delta_m^2 \quad \text{for} \quad \alpha \ll 1; \quad u^{\rm axi}(\phi) \sim \phi^2 \quad \text{for} \quad \alpha \gg 1. \tag{29}$$

The function $u^{\rm axi}(\phi)$ is depicted in Fig. 3 (blue line). Interestingly, as the confinement α becomes large, we find from Eq. (25) that $\varepsilon_{\theta\theta} + \varepsilon_{rr} \approx 0$, such that the area of the sheet is unchanged [Eq. 9(a)] . However, one should note that this invariance of the area is composed of significant stretching of radials and shrinking latitudes on the sheet, such that ε_{rr} and $\varepsilon_{\theta\theta}$ are both proportional to the geometric strain $\delta_g \sim (W/R)^2$. The corresponding stress profiles [Eq. (27)] are plotted in Fig. 4 (black curves). From the expression for $\sigma_{\theta\theta}^{\rm axi}$ one immediately obtains that the critical value at which a compressive zone emerges is $\alpha^*[\tilde{K} = \infty] = 8$.

As the coverage fraction ϕ increases, the (normalized) adhesion energy $u_{\rm ad} = \Gamma/(E_f t)$ becomes comparable to $u^{\rm axi}(\phi)$, and for $\phi > \phi_{\rm rig}$ delamination becomes energetically favorable in comparison to the axisymmetrically laminated state. This analysis shows that delamination is expected at high confinement, $\alpha \gg 1$; hence, we focus our analysis in this paper on this asymptotic parameter regime.

B. The deformability parameter

What happens when the substrate is not infinitely rigid? Since the profile $\zeta^{\rm axi}(r)$ is allowed to deviate from the ideal spherical shape, analytic solution to the FvK Eqs. (26) is not available, and we resort to numerical analysis (using an integration method similar to [34]). A few representative plots of the stresses and profiles are shown in Fig. 4. The characteristic behavior of the stress field remains valid also for finite values of $\tilde{K}$, whereby both radial and hoop components are tensile for sufficiently small confinement, and a hoop compression emerges above a critical value $\alpha^*(\tilde{K})$. The critical value $\alpha^*(\tilde{K})$ is defined by the implicit equation

$$\sigma_{\theta\theta}^{\rm axi}[r = W; \tilde{K}, \alpha^*(\tilde{K})] = 0. \tag{30}$$

For a nearly rigid substrate, $\tilde{K} \to \infty$, our numerical solution shows that $\alpha^*(\tilde{K}) \to 8$, in agreement with the above analytic result for the infinitely rigid substrate. In this limit, the substrate's spherical profile is barely deformed. However, as $\tilde{K}$ decreases, $\alpha^*(\tilde{K})$ increases. This trend is accompanied by

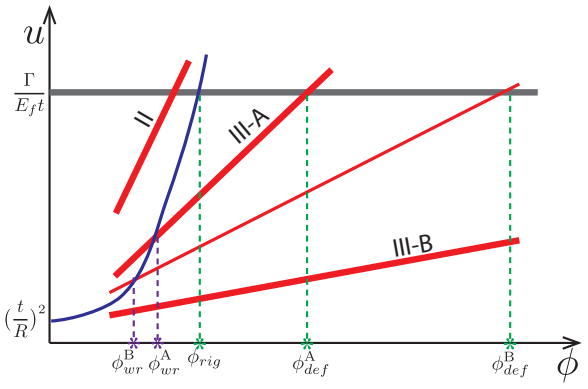

FIG. 3. (Color online) A schematic diagram comparing the various normalized energies upon increasing the coverage fraction ϕ: the energy of axisymmetric configuration, $u^{\rm axi}$, is described by the blue (thin black) parabola; the energetic cost of adhesion, $\Gamma/E_f t$, is described by the black (thick) horizontal line; and the two components of the wrinkle energy, $u^{\rm wr} = u^{\rm dom} + u^{\rm sub}$ [Eq. (33)], where $u^{\rm dom} \sim w_{\rm surf}$ is the tensile work done by the adhesive substrate pulling on the film [thin red (gray) line], which overrides the energy stored in the compression-free stress field [see Eqs. (48) and (50)], and $u^{\rm sub}$ is the energetic cost of bending and substrate deformation associated with the formation of wrinkles [Eq. (49b), thick red (gray) line]. A wrinkled state emerges at values of $\phi > \phi_{wr}$, where the axisymmetric state is compressive near the edge and the combination of bending and substrate deformation cost is sufficiently small. The energy component $u^{\rm sub}$ is plotted for parameter regimes II, III-A, and III-B. In regime II, $u^{\rm wr} \approx u^{\rm sub} \gg u^{\rm axi}$ for all coverages ϕ, and delamination occurs at $\phi = \phi_{\rm rig}$ when $u^{\rm axi}$ exceeds $\Gamma/E_f t$. In regime III-A $u^{\rm wr} \approx u^{\rm sub}$, wrinkling sets in at $\phi = \phi_{\rm wr}^A$, and delamination occurs at $\phi = \phi_{\rm def}^A$. In regime III-B, $u^{\rm wr} \approx u^{\rm dom}$ [thin red (gray) line], wrinkles emerge at $\phi_{\rm wr}^B$, and delamination is suppressed until a large coverage fraction $\phi_{\rm def}^B \sim O(1)$ is reached. The nonzero intercept of the energy $u^{\rm axi}$ reflects the (small) bending energy of a film with macro-scale curvature $1/R$.

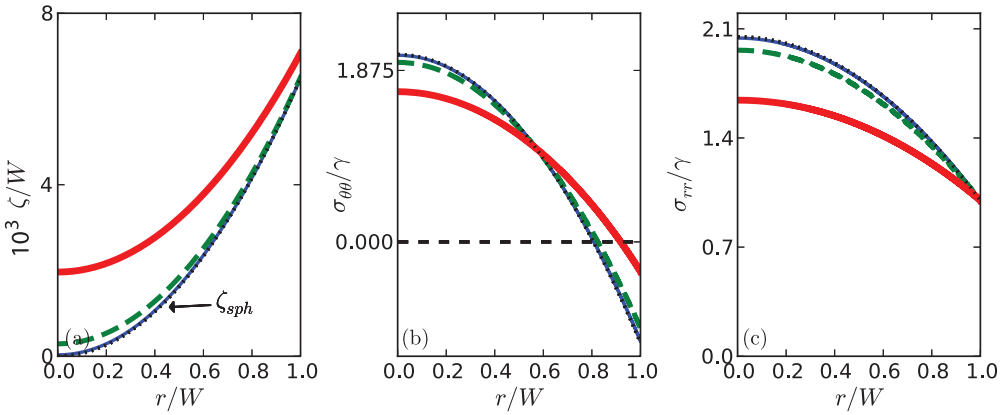

FIG. 4. (Color online) Plots of the shape $\zeta(r)$ and the stresses $\sigma_{rr}(r), \sigma_{\theta\theta}(r)$ in the unwrinkled, axisymmetric configuration for a fixed value of the confinement $\alpha \approx 17$ and a few representative values of $\tilde{K}$: $\tilde{K} = 1$ [red (solid gray) line], $\tilde{K} = 10$ [green (dashed gray) line], $\tilde{K} = 100$ [blue (solid black) line], and $\tilde{K} = \infty$ (dotted black line), in which case the vertical displacement of the plate is exactly $\zeta_{\rm sph}$ and the stress is given by the analytic solution, Eqs. (27).

the significant deformation of the substrate beneath the film, as can be observed in experiments of a film floating on a liquid drop [Fig. 1(c)].

In order to understand the effect of the deformability parameter $\tilde{K}$, it is useful to consider the energy $u^{\rm axi}$ of the axisymmetric state. Intuitively, if the substrate is not infinitely rigid, the strain, and hence the elastic energy $u^{\rm axi}$, may be reduced by flattening the substrate beneath the film such that the effective radius of curvature there becomes $R_{\rm eff} > R$. Such a mechanism is clearly instrumental for suppressing delamination of films from a liquid drop [35]. How soft must a substrate be in order that such a mechanism be operative? In the high confinement limit ($\alpha \gg 1$) we estimate the strain of an axisymmetric state by $\sim (W/R_{\rm eff})^2$ and the stretching energy is $u_{\rm strain} \sim (E_f t)(W/R_{\rm eff})^4$, favoring large $R_{\rm eff}$. The displacement from the original spherical shape is estimated as $\delta\zeta_{\rm sph} \sim W^2(1/R_{\rm eff} - 1/R)$, and the resulting substrate energy is $u_{\rm Win} \sim K\delta\zeta_{\rm sph}^2$. Comparing $u_{\rm strain}$ and $u_{\rm Win}$, we find that $R_{\rm eff} \approx R$ if the dimensionless deformability parameter $\tilde{K}^{-1} \ll 1$, hence we conclude that in this parameter range lamination yields only small deviations from the original spherical shape of the substrate. In contrast, regime I, which we define as [27]

$$\tilde{K} = KR^2/(E_f t) \ll 1, \tag{31}$$

is characterized by large distortion of the substrate. Accordingly, we expect that the scaling behavior of the energy $u^{\rm axi}$ is correctly described by Eq. (29) for $\tilde{K} \gg 1$, where $R_{\rm eff} \approx R$ and the substrate deformation energy is negligible. However, the energy $u^{\rm axi}$ in regime I, of highly deformable substrate, is significantly lower than the estimate (29), such that delamination could be avoided. In the rest of this paper we focus on the low-deformability regime, $\tilde{K} \gg 1$. The interesting physics of regime I will be addressed elsewhere [6].

IV. THE WRINKLED STATE

The wrinkling instability has been shown recently to hinder delamination of a uniaxially compressed film floating on a planar liquid surface [36]. Here we show that wrinkling should emerge even for a film attached to a curved, nearly rigid substrate. Furthermore, in the next section we show that the suppression of the elastic energy enabled by the formation of wrinkles has dramatic consequences on the delamination mechanism that could not be addressed by the 1D geometry of [36].

Recent studies of wrinkle patterns in thin films under tensile loads in 2D setups have employed the "far-from-threshold" (FT) method, a singular perturbation of FvK equations around a compression-free state of the film. The small parameter in the FT expansion is the inverse of the bendability parameter ϵ [Eq. (24)], which is the only dimensionless group that depends on the bending modulus. We implement the FT method, highlighting a unique aspect of the current work, a *doubly asymptotic* analysis of the wrinkle pattern, which involves both limits of high bendability ($\epsilon^{-1} \to \infty$) and large confinement $\alpha \to \infty$. Considering Fig. 5, which depicts a wrinkled laminated state, one may associate the first limit ($\epsilon^{-1} \to \infty$) as giving rise to divergence in the number of wrinkles and correspondingly to vanishing of their amplitude, and the second limit ($\alpha \to \infty$) with a maximal extension of their length, such that they occupy almost the whole sheet.

This type of asymptotic analysis, which corresponds to the parameter regime at which the wrinkle pattern becomes wrinklogami, namely, asymptotically isometric to the planar state of the film, distinguishes our work from those recent

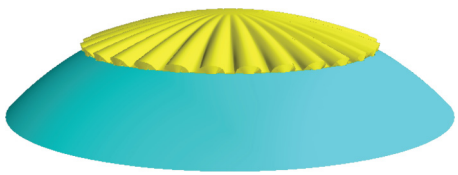

FIG. 5. (Color online) The wrinkled shape of a laminated film [yellow (light gray)] on a spherical substrate [blue (dark gray)]. The out-of-plane undulations of the film and the attached substrate are accompanied by in-plane oscillations of the perimeter of the film, which are of the same periodicity but with amplitude reduced by a factor of W/R. The amplitude of the wrinkles has been exaggerated to highlight their shape.

studies that addressed only the limit of high bendability ($\epsilon^{-1} \to \infty$) [29–31]. Understanding the doubly asymptotic limit is essential for our study, since we found above (Sec. III A) that it is the regime of large α where delamination may become energetically favorable.

A. Principles of the far-from-threshold expansion

Similarly to the classical Euler buckling of compressed rods, radial wrinkles relax the hoop confinement and enable the laminated film to attain a compression-free state whose energy u^{wr} is lower than the elastic energy u^{axi} of the compressed, axisymmetric (i.e., unwrinkled) state. Obviously, wrinkles require additional energy, due to the bending resistance of the film and the stiffness of the substrate. We evaluate the wrinkle energy u^{wr} by assuming the most basic wrinkled film-substrate shape [37],

$$\zeta(r,\theta) \approx \zeta_{\mathrm{sph}}(r) + f(r)\cos(m\theta), \tag{32a}$$

where $\zeta_{\mathrm{sph}}(r) \approx -r^2/R$ is the spherical profile, and the wrinkle amplitude $f(r)$ decreases as the sheet becomes thinner, or, more accurately, as the bendability ϵ^{-1} increases. Implicit in Eq. (32a) is our consideration of the low-deformability regime, $\tilde{K}^{-1} \ll 1$, where the nonoscillating part of the shape is approximated by the undeformed shape of the sphere. As we see below, the vertical displacement (32a) must be accompanied by radial and azimuthal displacements:

$$\mathrm{u}_r(r,\theta) = \mathrm{u}_r^{(0)}(r) + \mathrm{u}_r^{(m)}(r)\cos(m\theta), \tag{32b}$$

$$\mathrm{u}_\theta(r,\theta) = \mathrm{u}_\theta^{(2m)}(r)\sin(2m\theta). \tag{32c}$$

The displacement field, represented in Eqs. (32) by the functions $f(r), \mathrm{u}_r^{(0)}(r), \mathrm{u}_r^{(m)}(r), \mathrm{u}_\theta^{(2m)}$, is found as a singular FT expansion of FvK equations (17) [8,29]. In this approach, we expand the FvK equations around the singular limit of infinite bendability ($\epsilon \to 0$). Namely, the energy u^{wr} of the wrinkled state is assumed to have the form

$$u^{\mathrm{wr}} = u^{\mathrm{dom}} + u^{\mathrm{sub}}, \tag{33}$$

where

$$u^{\mathrm{sub}}/u^{\mathrm{dom}} \approx g(\tilde{K},\alpha)\cdot\epsilon^{\beta} \quad \text{for} \quad \epsilon \to 0, \tag{34}$$

with $g(\tilde{K},\alpha)$ some unknown function and $\beta > 0$. Here, u^{dom} is the "dominant" energy stored in the asymptotic, compression-free stress field, which consists of the straining energy u_{strain} [Eq. (16)] and the work w_{surf} of the tensile load at the edge of the film [Eq. (10)]; this energy term depends only on the "macroscopic" parameters $\tilde{K}^{-1}$ and α and bares no explicit dependence on the bendability ϵ^{-1} or any small-scale features of the wrinkle pattern. In contrast, the energy u^{sub} is the "subdominant" energy which depends on the wrinkle number m and amplitude $f(r)$ and is determined by a balance of bending and substrate stiffness.

It is crucial to emphasize a simple yet somewhat confusing point: The FT relation (34) means that if the confinement α (as well as $\tilde{K}$) is held fixed, and the bendability ϵ^{-1} increases indefinitely, then the energy u^{sub} becomes smaller than u^{dom} for sufficiently small ϵ. This basic feature, which was noted in previous FT studies of wrinkle patterns [29], motivated the usage of the notations "dom" and "sub" for the respective energy terms. However, when analyzing the doubly asymptotic limit ($\alpha \to \infty$ and $\epsilon^{-1} \to \infty$), of both confinement and bendability parameters, we must pay special attention to the prefactor $g(\tilde{K},\alpha)$ in Eq. (34). We show that $g(\tilde{K},\alpha)$ vanishes for large α. As a conclusion, we must take into consideration the counterintuitive possibility that the energy term u^{sub} may actually be larger than u^{dom}.

The above paragraph highlights a potential source of confusion in our analysis, since it requires the implementation of the FT formalism—an expansion in the inverse bendability ϵ—to situations where another independent parameter (the confinement α) becomes asymptotically large. We thus need to clarify the meaning of adjectives such as "finite," "diverging," and "vanishing." Unless specifically stated otherwise, we use the symbol "$\to$" to denote the limit $\epsilon \to 0$ (for fixed values of the parameters $\tilde{K}$ and α) and will attribute the above adjectives to the asymptotic behavior in this limit. For instance, we refer to the energy u^{dom} as "finite" since it approaches the ϵ-independent limit as $\epsilon \to 0$, and to u^{sub} as "vanishing" since it scales $\sim\epsilon^{\beta}$ as $\epsilon \to 0$, but this terminology does not mean that $u^{\mathrm{dom}} > u^{\mathrm{sub}}$ at a given pair of values of ϵ and α. Another important example pertains to the amplitude of wrinkles and their number. The amplitude $f(r)$ is vanishing and the number m is diverging, whereas their product $mf(r)$ approaches a finite (i.e., ϵ-independent) limit, which is necessary to collapse the compression in the azimuthal direction. Other, more obvious, examples of finite objects, are the axisymmetric component of the radial displacement $\mathrm{u}_r^{(0)}(r)$, the fixed slope $\frac{d}{dr}\zeta_{\mathrm{sph}}$, and the radial strain ε_{rr}.

The basic structure of this far-from-threshold expansion appeared already in [29], which considered radial wrinkles in a planar (Lamé) setup, and its singular nature was elaborated in [30]. However, the displacement field (32) differs from that study by the existence of an axisymmetric contribution ζ_{sph} to the out-of-plane displacement field and by the related, harmonic contribution $\mathrm{u}^{(m)}(r)\cos(m\theta)$ to the radial displacement. In the following sections we derive the dominant and subdominant energies and highlight the unique aspects of the wrinkled state in this problem.

B. The compression-free stress field

For the specific system we address here, of a circular film attached to a spherical substrate, the compression-free field and its associated energy u^{dom} have been calculated analytically in the limit $\tilde{K} \to \infty$ of an infinitely rigid substrate [31]. Therefore, in this section we briefly describe this result and refer the reader to [31] for a detailed calculation.

Since very thin films cannot support compression, the stress field that underlies the wrinkle pattern (often called the "membrane" limit [22]) is assumed to satisfy $\sigma_{ii} \geqslant 0$ in the high bendability limit $\epsilon \to 0$, where i labels the two principal directions of the stress tensor [38–40]. This principle is also known as "tension field theory" [22,38,40] or "relaxed energy" [39]. For our laminated, axially loaded film, this condition is naturally realized by solving the force balance Eqs. (26) in two distinct zones: an inner one ($0 < r < L$) and an outer one ($L < r < W$), separated at some radius $r = L$, where appropriate matching conditions are invoked [41].

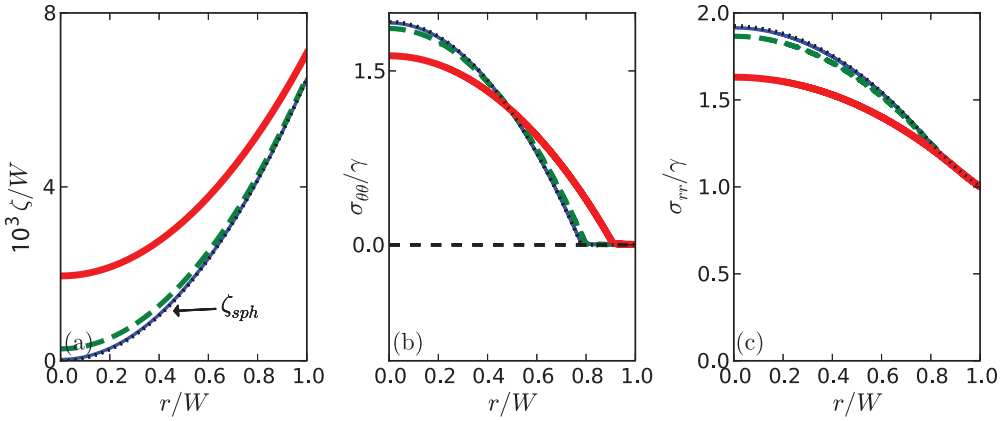

FIG. 6. (Color online) Plots of the shape $\zeta(r)$ and the stresses $\sigma_{rr}(r)$,$\sigma_{\theta\theta}(r)$ in the wrinkled configuration for a fixed value of the confinement $\alpha \approx 17$ and a few representative values of $\tilde{K}$: $\tilde{K} = 1$ [red (solid gray) lines], $\tilde{K} = 10$ [green (dashed gray) lines], $\tilde{K} = 100$ [blue (solid black) lines], and $\tilde{K} = \infty$ (dotted black lines), in which case the (nonoscillatory) vertical displacement of plate is exactly $\zeta_{\rm sph}$ and the stress is given by the analytic solution, Eqs. (36)–(38).

In the inner disk, $(0 < r < L)$, both radial and hoop stresses are purely tensile, and are described by the corresponding stress $\sigma^{\rm axi}(r;\tilde{K},\alpha)$ of the axisymmetric state, upon replacing

$$W \to L, \quad \gamma \to \sigma_{rr}(L), \quad \alpha \to \overline{\alpha} = \frac{(E_f t)}{\sigma_{rr}(L)}\left(\frac{L}{R}\right)^2. \tag{35}$$

In particular, in the limit $\tilde{K} \to \infty$, the axisymmetric stress field is given analytically by Eq. (27), such that

$$(0 < r < L): \quad \frac{\sigma_{\theta\theta}(r)}{\sigma_{rr}(L)} = \frac{1}{16}\overline{\alpha}\left[1 - 3\left(\frac{r}{L}\right)^2\right] + 1, \tag{36a}$$

$$(0 < r < L): \quad \frac{\sigma_{rr}(r)}{\sigma_{rr}(L)} = \frac{1}{16}\overline{\alpha}\left[1 - \left(\frac{r}{L}\right)^2\right] + 1. \tag{36b}$$

In the outer annulus, $L < r < W$, where wrinkles emerge, the radial stress is still tensile ($\sigma_{rr} > 0$) and finite, whereas both $\sigma_{\theta\theta}$ and $\sigma_{r\theta}$ are negligible, namely vanish as $\epsilon \to 0$. The radial stress is thus immediately obtained from Eq. (26) by using the BC $\sigma_{rr}(W) = \gamma$, obtaining

$$(L < r < W): \quad \sigma_{rr} \to \gamma W/r, \quad \sigma_{\theta\theta} \to 0. \tag{37}$$

The length L and the stress $\sigma_{rr}(L)$ are determined by requiring continuity of σ_{rr} and $\sigma_{\theta\theta}$ at the borderline $r = L$. This implies that the effective confinement $\overline{\alpha}$ [Eq. (35)] felt by the inner disk is just at the critical value $\alpha^*(\tilde{K})$. We thus obtain

$$L = W\left[\frac{\alpha^*(\tilde{K})}{\alpha}\right]^{1/3}, \quad \sigma_{rr}(L) = \gamma\left[\frac{\alpha}{\alpha^*(\tilde{K})}\right]^{1/3}. \tag{38}$$

As the confinement increases, $\alpha \gg \alpha^*(\tilde{K})$, we find that L decreases indefinitely and the wrinkled annulus thus occupies most of the laminated area of the substrate [42].

Figure 6 shows the numerical solution for the shape and the compression-free stress field for various values of $\tilde{K}$ and compares them with the analytic solution for $\tilde{K} \to \infty$, Eqs. (36) and (37), where the shape $\zeta(r) \to \zeta_{\rm sph}(r)$.

C. Asymptotic displacement and strain

The analysis in Sec. IV B suffices to compute the energy term $u^{\rm dom}$ in Eq. (33). In order to evaluate $u^{\rm sub}$ it is essential for us to discuss first a few constraints on the displacement field, Eq. (32), which are imposed by the requirement that the stress approaches the compression-free field [Eqs. (36) and (37)].

Our analysis of the compression-free stress field assumed that in the wrinkled zone $L < r < W$, both hoop and shear stresses vanish: $\sigma_{\theta\theta},\sigma_{r\theta} \to 0$ as $\epsilon \to 0$. Compatibility of these conditions with the Hookean stress-strain relations, Eq. (4), imposes two conditions on the strain tensor in the limit $\epsilon \to 0$,

$$\varepsilon_{r\theta} \to 0, \tag{39}$$

$$\varepsilon_{\theta\theta} \to -\Lambda\varepsilon_{rr}, \tag{40}$$

where the radial strain ε_{rr} is readily obtained from Eqs. (37) and (4):

$$\varepsilon_{rr} = \sigma_{rr}/(E_f t) \to \frac{\gamma}{(E_f t)}\frac{W}{r}. \tag{41}$$

Similarly to the axisymmetric state [Eq. (25)], we find that the areal change of the wrinkled film $dA_{\rm fil}$, Eq. (9a), approaches zero in the large confinement $\alpha \to \infty$. However, in contrast to the axisymmetric case, here this property truly indicates the asymptotic isometry of the wrinkled state in this limit, since it stems from the simultaneous suppression of *every* component of the strain tensor.

Considering now the geometric link between strain and displacement, Eq. (3), we can characterize numerous components of the displacement field (32).

Radial strain. For the axisymmetric component $\mathrm{u}_r^{(0)}$ of the radial displacement we obtain, using Eqs. (3a) and (41),

$$\frac{d}{dr}\mathrm{u}_r^{(0)} + \frac{1}{2}\left(\frac{d}{dr}\zeta_{\rm sph}\right)^2 \to \frac{\gamma}{(E_f t)}\frac{W}{r}, \tag{42}$$

where $(\frac{d}{dr}\zeta_{\rm sph})^2 \sim (r/R)^2$. The geometric meaning of this equation is elucidated by considering the infinite confinement limit $\alpha = \delta_g/\delta_m \to \infty$, where the isometric mapping of radial lines on the curved sphere (namely, $\varepsilon_{rr} = 0$) is obtained by radial displacement $\mathrm{u}_r^{(0)}(r) \approx -\int_0^r \frac{d}{dr}(\zeta_{\rm sph})^2/2 \approx -r^3/6R^2$. Hence, in the large confinement limit the radial displacement $\mathrm{u}_r^{(0)}$ is dominated by the geometric strain $\delta_g = (W/R)^2$, rather than by the mechanical strain $\frac{\gamma}{(E_f t)}\frac{W}{r} \sim \delta_m$.

Hoop strain. For the axisymmetric component of the hoop strain we obtain, using Eqs. (3b) and (40),

$$\frac{\mathrm{u}_r^{(0)}}{r}+\frac{m^2}{4r^2}f^2\to\Lambda\frac{\gamma}{(E_f t)}\frac{W}{r}. \tag{43}$$

The geometric meaning of this equation, whose analog in [29,30] was dubbed *slaving condition*, is that the fraction of latitudinal length absorbed by the wrinkle undulations $[m^2 f(r)^2/4r^2]$ together with the shrinkage of latitudes $(\mathrm{u}_r^{(0)}/r)$ must equal the appropriate hoop strain $[\varepsilon_{\theta\theta}\to-\Lambda\varepsilon_{rr}$, Eq. (40)] that is necessary for the collapse of hoop compression $(\sigma_{\theta\theta}\to 0)$. Considering again the large confinement limit, $\alpha\gg 1$, we note that in contrast to wrinkle patterns on a planar background [29], where all three terms in Eq. (43) are comparable, the large confinement regime addressed by our study is characterized by the balance of the two terms on the left side of Eq. (43), which both scale with δ_g, whereas the term on the right is much smaller, scaling with the mechanical strain $\delta_m\ll\delta_g$. Thus, similarly to $\mathrm{u}_r^{(0)}$, the product mf is determined in the large confinement limit by the geometric strain $\delta_g\sim(W/R)^2$, rather than by the mechanical strain $\delta_m\sim\gamma/(E_f t)$.

The oscillating component of the hoop strain $\varepsilon_{\theta\theta}$ [namely, the part of Eq. (3b) that is $\propto\sin(2m\theta)$] yields an additional equation:

$$\frac{2m}{r}\mathrm{u}_\theta^{(2m)}-\frac{m^2}{4r^2}f^2=0. \tag{44}$$

This equation for the azimuthal displacement $\mathrm{u}_\theta^{(2m)}$ is necessary to eliminate a highly energetic oscillating component of the hoop stress, but it will not be required for the evaluation of the energy u^{sub}.

Shear strain. Finally, the shear strain $\varepsilon_{r\theta}$ has only an oscillating component $\propto\cos(m\theta)$, for which we obtain, using Eqs. (3c) and (39):

$$\frac{m}{r}\mathrm{u}_r^{(m)}+\frac{m}{r}f\frac{d}{dr}\zeta_{\mathrm{sph}}\to 0. \tag{45}$$

Similarly to Eq. (44), which determines the azimuthal displacement required to eliminate a finite amount of oscillating hoop stress, Eq. (45) determines an oscillating component of the radial displacement $\mathrm{u}_r^{(m)}\cos(m\theta)$ that is required to eliminate a finite *shear stress* [43]. In other words, the out-of-plane undulations which relax the compressive hoop stress, must be accompanied by in-plane oscillations of the boundary of the same periodicity $(2\pi/m)$ and of comparable amplitude $(\mathrm{u}_r^{(m)}\sim f)$. A similar effect was noted in [44] in a problem of metric-generated cascades.

D. Wrinklogami: Asymptotic isometry assisted by wrinkles

Our analysis of the compression-free stress (Sec. IV B) and the displacement field (Sec. IV C) allows us to evaluate the energy u^{wr} of the wrinkled state. This analysis will reveal the nontrivial isometry attained by the wrinkle pattern in the doubly asymptotic regime of high bendability and large confinement $(\epsilon^{-1},\alpha\gg 1)$ and will enable us to identify the sector in the parameter space at which the laminated state becomes wrinkled.

1. Evaluating the wrinkle energy

In the FT expansion, the wrinkle energy u^{wr} is decomposed into two components [Eq. (33)]. As we explained in Sec. IV A, the energy u^{dom} is stored in the compression-free stress field and the work done on the film by the adhesive substrate and approaches a finite value $u^{\mathrm{dom}}(\alpha,\tilde{K})$ in the high-bendability limit $\epsilon\to 0$. We show below that $u^{\mathrm{dom}}(\alpha,\tilde{K})$ actually vanishes as $\alpha\to\infty$. In contrast, the energy u^{sub} is associated with the energetic costs of bending the sheet and deforming the substrate due to the azimuthal undulations of wrinkles. The FT expansion requires the energy u^{sub} to vanish as $\epsilon\to 0$ [29], but we show that it may override u^{dom} in a subdomain of the doubly asymptotic regime $\epsilon^{-1},\alpha\gg 1$.

Evaluating u^{dom}. The energy u^{dom} [where normalization is, per our convention, by $(E_f t)W^2$] is the sum of the straining energy [Eq. (16)], evaluated for the compression-free stress field, and the work $w_{\mathrm{surf}}=-\gamma dA_{\mathrm{sph}}/(E_f t)W^2$ [Eq. (10)]. In order to evaluate these contributions, we consider the limit $\tilde{K}\to\infty$, where we can use the analytic expressions obtained above, Eqs. (36)–(38) and Eq. (42), to obtain a well-defined, $\tilde{K}$-independent expression that we denote as $u^{\mathrm{dom}}(\alpha)$. For sufficiently small values of $\tilde{K}^{-1}$, we use this value to approximate $u^{\mathrm{dom}}(\alpha,\tilde{K})$.

We evaluate the straining energy u_{strain} by dividing the integral in Eq. (16) to two parts: $\int_0^W=\int_0^L+\int_L^W$. For the first part, where the film is unwrinkled, we use Eq. (28), replacing $W\to L$, $\gamma\to\sigma_{rr}(L)$, and $\alpha\to\alpha^*$ and using Eqs. (38) for L and $\sigma_{rr}(L)$, substituting $\alpha^*=8$. For the second part, where the film is wrinkled, we substitute in the integral the only nonvanishing component of the compression-free stress field: $\sigma_{rr}=\gamma W/r$. We thus obtain

$$u_{\mathrm{strain}}=\pi\delta_m^2\left[\frac{1}{6}(7-6\Lambda)+\log\left(\frac{\alpha}{\alpha^*}\right)^{1/3}\right]. \tag{46}$$

For the work w_{surf}, we use Eqs. (10) and (42) and obtain

$$w_{\mathrm{surf}}=\frac{\bar{\mathrm{W}}_{\mathrm{surf}}}{(E_f t)W^2}=\pi\delta_m^2\left[\alpha+8\left(-4+3\Lambda+\log\frac{\alpha}{\alpha^*}\right)\right]. \tag{47}$$

Considering the contributions from Eqs. (46) and (47), we notice that in the limit of large confinement $(\alpha=\phi/\delta_m\gg 1)$ the energy u^{dom} is governed by the work of the adhesive force pulling on its edge. Namely, $w_{\mathrm{surf}}\gg u_{\mathrm{strain}}$, and hence,

$$u^{\mathrm{dom}}\approx w_{\mathrm{surf}}\sim\delta_m\phi. \tag{48}$$

The linear dependence of the energy component u^{dom} on the laminated fraction ϕ is depicted by the red thin curve in Fig. 3. The negligibility of the energy u_{strain} in comparison to the work w_{surf}, reflects the *asymptotic isometry* attained by the wrinkle pattern in the doubly asymptotic limit of large confinement, $\alpha\gg 1$, and high bendability, $\epsilon^{-1}\gg 1$. In Sec. VI B we elaborate further on the importance of this result.

Evaluating u^{sub}. Let us turn now to the energy u^{sub}. In Appendix B we generalize the scaling analysis of [31] for large confinement values, and show that in the low-deformability regime $(\tilde{K}^{-1}\ll 1)$ the wrinkle number is determined by a balance between the azimuthal bending force $\sim B(m^4/r^4)f$

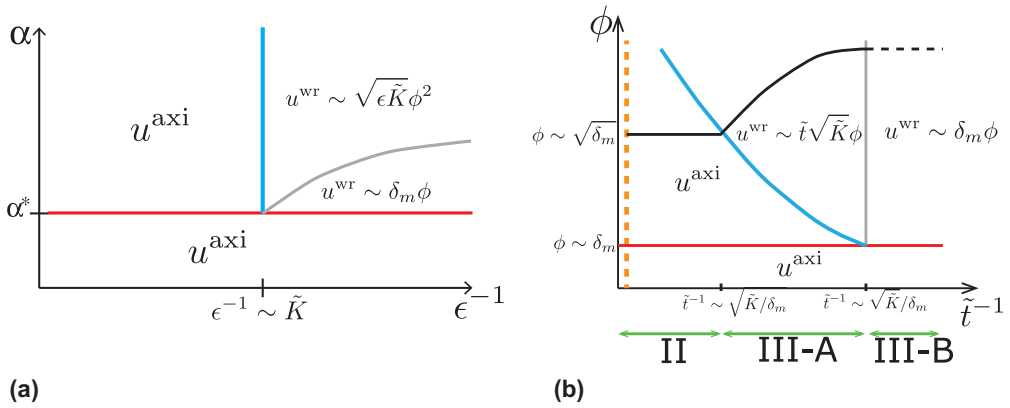

FIG. 7. (Color online) (a) The behavior of the laminated states in the bendability-confinement plane (ϵ^{-1},α). Here we assume that the sheet is sufficiently thin such that the bendability is high ($\epsilon \ll 1$), and consider a fixed, small value of the deformability parameter $\tilde{K}^{-1} \ll 1$. The horizontal red (thick gray) line $\alpha = \alpha_c(\tilde{K})$ corresponds to the critical confinement below which the tensile (adhesive) force γ exerted at the edge of the sheet is sufficiently strong that the sheet is under pure tension. The vertical blue (thick gray) line $\epsilon^{-1} \approx \tilde{K} \gg 1$ (where $\epsilon = \epsilon_g$) corresponds to the minimal bendability value for which the energetic cost $u^{\rm sub}$ of bending and substrate deformation makes the wrinkled state energetically favorable in comparison to the axisymmetric (compressed, unwrinkled) state. The thin gray curve separates two parts of the parameter regime at which a wrinkle pattern is energetically favorable for the laminated state. Above this curve, the energy $u^{\rm sub}$ [Eq. (49b)] of bending and substrate deformation governs the energy $u^{\rm wr}$ of the wrinkled state. Below the thin gray curve, bendability is sufficiently large and the wrinkle energy is governed by the energy $u^{\rm dom}$ [Eq. (48)], associated with the work done by the tensile load at the film's edge. (b) Replotting the diagram in panel (a), where we replace the bendability and confinement parameters ϵ^{-1} and α with the pristine dimensionless parameters of thickness $\tilde{t} = t/R$ and coverage fraction $\phi = (W/R)^2$, and consider fixed, small values of the deformability parameter $\tilde{K}^{-1} \ll 1$ and of the mechanical tension $\delta_m \ll 1$. The solid gray curves correspond to the respective curves in panel (a). The black curve marks the threshold $\phi_{\rm def}$ above which delamination is energetically favorable, and the vertical dashed orange (gray) line marks the maximal value of $\tilde{t}$, above which the film does not delaminate. The green (gray) double arrows show the parameter regimes that we call, respectively, II, III-A, and III-B (regime I, which corresponds to sufficiently soft substrate, i.e., $\tilde{K} \ll 1$, is not shown in this figure). If $\sqrt{\delta_m/\tilde{K}} < \tilde{t} < \sqrt{\delta_m}$, the system is at regime II, where the energetically favorable laminated state is axisymmetric (compressed, unwrinkled), and delamination becomes favorable for $\phi > \phi_{\rm rig}$ [Eq. (1)]. If $\tilde{t} < \sqrt{\delta_m/\tilde{K}}$, the system is at parameter regime III, where the film becomes wrinkled at $\phi > \phi_{\rm wr}$ and delamination becomes energetically favorable for $\phi > \phi_{\rm def}$, where $\phi_{\rm wr}, \phi_{\rm def}$ are given by Eqs. (55) and (56).

and the substrate restoring force Kf. This balance means that the energy $u^{\rm sub}$ is governed by the sum of two comparable contributions, of the energies $u_{\rm bend}$ and $u_{\rm Win}$, which can be evaluated, respectively, from Eqs. (15) and (13). We evaluate these energies by noting that the product $m^2 f^2$ is subjected to the slaving condition, Eq. (43), which implies $m^2 f^2 \sim r^4/R^2$ in the doubly asymptotic limit $(\epsilon^{-1},\alpha \gg 1)$. These considerations yield the following estimates of the wrinkle number m and the energy $u^{\rm sub}$,

$$m \sim \left(\frac{KW^4}{B}\right)^{1/4} \sim \left(\frac{\tilde{K}}{\epsilon}\right)^{1/4}, \tag{49a}$$

$$u^{\rm sub} \sim \frac{B}{(E_f t)W^2}\int_0^W \frac{m^4 f^2}{r^4} r dr$$

$$\sim \sqrt{\epsilon \tilde{K}}\phi^2 \sim \tilde{t}\sqrt{\tilde{K}}\phi, \tag{49b}$$

where the bendability parameter is $\epsilon^{-1} = \epsilon_g^{-1}$, as defined in Eq. (24). Note that the first expression for $u^{\rm sub}$ in Eq. (49b) does not reveal the actual ϕ dependence of this energy when all "pristine" parameters in Eqs. (20) and (21), except ϕ, are held fixed. Expressing $\epsilon = \epsilon_g$ [Eq. (24)] through ϕ and $\tilde{t}$, we obtained the last expression, which shows that in such an analysis, the energy $u^{\rm sub}$ increases linearly with ϕ. This linear dependence is illustrated in Fig. 3 (red thick line) for various parameter regimes.

2. *The energy of a laminated state*

The above evaluation of the energy terms $u^{\rm dom}$ and $u^{\rm sub}$ shows that in the high-bendability, large-confinement, low-deformability regime $(\epsilon^{-1},\alpha,\tilde{K} \gg 1)$, the energetic cost of strain is negligible, and the wrinkle energy is thus described by

$$u^{\rm wr} \approx w_{\rm surf} + u^{\rm sub}, \tag{50}$$

where $u^{\rm sub} = u_{\rm bend} + u_{\rm Win}$ is governed by the bending modulus B and the substrate stiffness K, and the work $w_{\rm surf}$ is proportional to the tension γ exerted on the film's boundary. Remarkably, the energy $u_{\rm strain}$ does not appear in this expression, nor does the stretching modulus $Y = (E_f t)$. This fact is a direct consequence of the collapse of all components of the strain tensor [Eqs. (39)–(41)] and reflects the asymptotic isometry exhibited by the wrinkled state [Eq. (32)] in the limit $(\epsilon^{-1},\alpha \to \infty)$ for some $\tilde{K} \gg 1$.

The two parts of the energy of the wrinkled state, $w_{\rm surf}$ and $u^{\rm sub}$, are plotted in Fig. 3 as linear functions of the coverage fraction ϕ for some given value of the mechanical strain parameter δ_m. Here $w_{\rm surf}$ is depicted by a single thin red line, whose slope is $\sim\delta_m$, and thick red lines are used to depict the behavior of $u^{\rm sub}$, for three ranges of the product $\tilde{t}\sqrt{\tilde{K}}$. For $\tilde{t}\sqrt{\tilde{K}} \ll \delta_m$, we can approximate the wrinkle energy by the thin red line (i.e., $u^{\rm wr} \approx w_{\rm surf}$, regime III-B), whereas for $\tilde{t}\sqrt{\tilde{K}} \gg \delta_m$, the wrinkle energy can be approximated by

the corresponding thick red line (i.e., $u^{\rm wr} \approx u^{\rm sub}$, regimes II and III-A). Next we use these evaluations of the energy $u^{\rm wr}$ to compare with the energy $u^{\rm axi}$ of the axisymmetric (unwrinkled) state. This comparison allows us to evaluate the characteristic values at which the film becomes wrinkled ($\phi_{\rm wr}$) and delaminates from the substrate ($\phi_{\rm rig}$ or $\phi_{\rm def}$) in each of these parameter regimes.

Considering the energies $u^{\rm axi}$ of the unwrinkled state [Eq. (29)] and the wrinkle energy $u^{\rm wr}$ [Eq. (50)], we find that the mechanics of a laminated state is governed by the three dimensionless groups: bendability ϵ^{-1}, confinement α, and deformability $\tilde{K}^{-1}$. This is shown in Fig. 7(a), which plots schematically the morphology and energy of the laminated state as ϵ^{-1} and α are varied, for a fixed value of $\tilde{K}$. If $\alpha < \alpha^*(\tilde{K}) \approx 8$, the laminated state is under pure tension, and the axisymmetric state is the stable laminated configuration. If $\epsilon^{-1} \ll \tilde{K}$, the substrate is too rigid and the wrinkle energy is too large, making the wrinkled state unfavorable in comparison to a compressed (unwrinkled) axisymmetric state. The parameter regime $\left[\alpha \gg \alpha^*(\tilde{K}), \epsilon^{-1} \gg \tilde{K}\right]$, where the wrinkle pattern is energetically favorable in comparison to the axisymmetric state, splits into two subdomains: $\alpha \ll (\epsilon\tilde{K})^{-1/2}$, where the wrinkle energy is governed by the work of adhesion, such that $u^{\rm wr} \sim w_{\rm surf}$ (corresponding to regime III-B in Fig. 3); and $\alpha \gg (\epsilon\tilde{K})^{-1/2}$, where the wrinkle energy is governed by bending and substrate deformation, such that $u^{\rm wr} \sim u_{\rm bend} + u_{\rm Win}$ (corresponding to regimes II and III-A in Fig. 3).

V. PROLAMINATION BY WRINKLING

The energy evaluations in the previous two sections allow us to determine the energetically favorable state: laminated-unwrinkled [$u = u^{\rm axi}$, Eq. (29)], laminated-wrinkled [$u = u^{\rm wr}$, Eqs. (50), (48), (49b)], or delaminated ($u = \Gamma/E_f t$). In this section we perform this energetic comparison, starting with the Winkler foundation, and then generalizing the results for an adhesive film on a compliant spherical substrate. Let us recall the simplifying assumption, $\Gamma \approx \gamma$ [Eq. (22)], that we make in the current study. The general case ($\Gamma \neq \gamma$) will entail the appearance of the ratio Γ/γ in the various formulas, but should not affect the scaling laws derived in this section.

A. Winkler foundation

In order to facilitate the comparison of energies, it is useful to transform the coordinates ϵ^{-1} and α in Fig. 7(a) to $\tilde{t}^{-1}$ and ϕ. The new diagram is depicted in Fig. 7(b), where the red, blue, and gray curves are mapped from their counterparts in Fig. 7(a) by using the parameter transformation: $\epsilon \to (\tilde{t}/\phi)^2$; $\alpha \to \phi/\delta_m$ [Eqs. (20), (23), and (24)]. An additional curve (black) in Fig. 7(b) marks the maximal value of ϕ, above which the energy of the laminated state becomes larger than the energetic cost of delamination $\gamma/(E_f t) = \delta_m$ [where we normalize energy, as usual, by $(E_f t)W^2$, and use the simplifying assumption, Eq. (22)]. For completeness of our description, we added one more vertical curve (orange), which corresponds to the maximal value of the thickness parameter $\tilde{t} \sim \sqrt{\delta_m}$, above which lamination is never favorable (see Sec. II B 4).

For a given pair of mechanical tension and deformability $(\delta_m, \tilde{K})$, Fig. 7(b) allows us to distinguish between the following parameter regimes.

(i) *Regime II, where* $\sqrt{\delta_m/\tilde{K}} < \tilde{t} < \sqrt{\delta_m}$. In this regime, the laminated state of the film is always axisymmetric (unwrinkled), and delamination occurs at $\phi = \phi_{\rm rig} = \sqrt{\delta_m}$. In dimensional units this parameter regime corresponds to

$$K > K_{\rm rig}, \quad \text{where} \quad K_{\rm rig} \sim \Gamma/t^2. \tag{51}$$

Recalling Eq. (31), we may express regime I, where the substrate is highly deformable [and is not included in Fig. 7(b)], through dimensional units, by identifying another characteristic stiffness:

$$K < K_{\rm soft}, \quad \text{where} \quad K_{\rm soft} \sim (E_f t)/R^2. \tag{52}$$

The characteristic stiffness values $K_{\rm soft}$ and $K_{\rm rig}$, lead us to define the intermediate parameter regime III, $K_{\rm soft} < K < K_{\rm rig}$, which splits into two parts, as shown in Fig. 7(b).

(ii) *Regime III-A, where* $\delta_m/\sqrt{\tilde{K}} < \tilde{t} < \sqrt{\delta_m/\tilde{K}}$. In dimensional units, regime III-A corresponds to

$$\frac{\gamma^2}{E_f t^3} < K < K_{\rm rig}. \tag{53}$$

In this regime, the film becomes wrinkled at

$$\phi_{\rm wr} \sim \tilde{t}\sqrt{\tilde{K}} = \sqrt{tK/E_f}, \tag{54a}$$

and delamination occurs at

$$\phi_{\rm def} \sim \sqrt{\frac{\delta_m}{\tilde{K}\tilde{t}^2}} = \sqrt{\frac{\gamma}{Kt^2}}, \tag{54b}$$

(iii) *Regime III-B, where* $\tilde{t} < \delta_m/\sqrt{\tilde{K}}$. In dimensional units, regime III-B corresponds to

$$K_{\rm soft} < K < \frac{\gamma^2}{E_f t^3}. \tag{55}$$

In this regime, the film becomes wrinkled at

$$\phi_{\rm wr} \sim \delta_m = \gamma/E_f t, \tag{56a}$$

and delamination occurs at

$$\phi_{\rm def} \sim O(1). \tag{56b}$$

The last equation implies that, at least in the small-slope approximation used in this study (i.e., $W/R \ll 1$), the film is sufficiently thin such that it can wrinkle so easily that delamination is not energetically favorable even at arbitrarily large coverage fractions.

Importantly, both parts of the intermediate-stiffness regime III are included in the low-deformability regime ($K > K_{\rm soft}$), and therefore wrinkling involves no macro-scale deformation of the substrate's shape. We call this phenomenon *prolamination*, where the maximally laminated coverage fraction increases while the substrate retains its curved shape. Noticing that $K_{\rm rig}/K_{\rm soft} \sim (\gamma R^2/E_f t)$, we expect the parameter regime III to become particularly noticeable when the effective thickness t/R decreases [Fig. 2(a)]. In other words, prolamination should become a predominant phenomenon in the adhesion of ultrathin films on curved substrates.

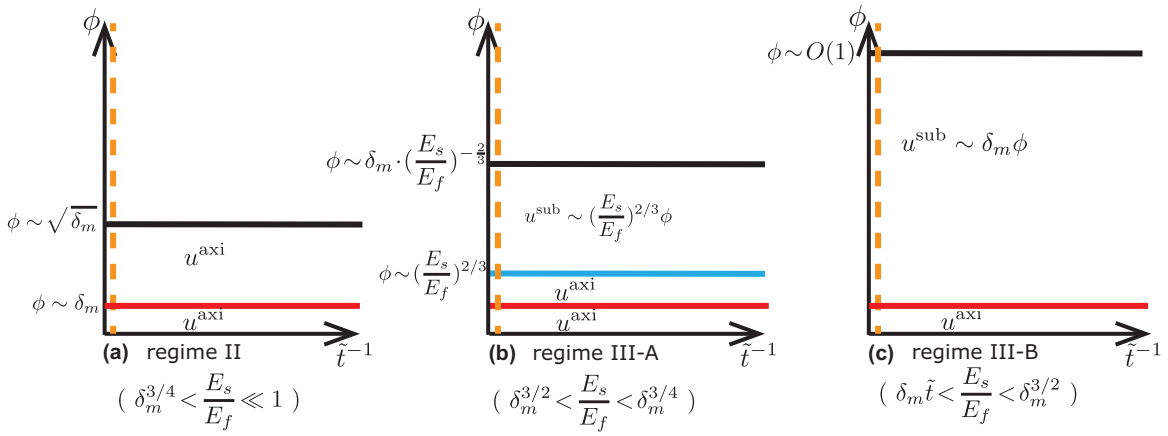

FIG. 8. (Color online) Diagrams analogous to Fig. 7(b), where the spherical substrate is assumed to be an isotropic solid of Young's modulus E_s (instead of stiffness K). The two parameter axes are $\tilde{t}^{-1}$ and ϕ, as in Fig. 7(b), and the parameters with small, fixed values are now $\delta_m = \gamma/E_f t$ [as in Fig. 7(b)] and the ratio (E_s/E_f) between the Young's moduli of the substrate and the film. Rather than a single diagram, we find it easier to plot here three separate diagrams [47], for three characteristic values of E_s/E_f, which correspond, respectively, to (a) regime II; (b) regime III-A; and (c) regime III-B. Similarly to Fig. 7(b), regime I, which corresponds to sufficiently soft substrate, $E_s < E_{s,\rm soft}$, is not shown here.

Our model system has four dimensionless groups: $\phi, \delta_m, \tilde{K}, \tilde{t}$ [Eqs. (20) and (21), assuming $\gamma/\Gamma = 1$]. The schematic Fig. 7(b) is essentially a planar section, where the full 4D phase diagram of the model is projected onto a 2D hyperplane spanned by the parameters ϕ and $\tilde{t}^{-1}$ (for fixed values of $\tilde{K}$ and δ_m). The schematic phase diagram in Fig. 2(a) is another projection of the 4D parameter space onto a hyperplane spanned by the dimensionless parameters KR/E_f and $\Gamma/E_f R$, none of which depends on the thickness of the film or the coverage fraction ϕ. The purpose of Fig. 2(a) is to describe the various scenarios that the system undergoes upon increasing ϕ, for various values of the substrate stiffness and curvature, and the strength of adhesion.

B. From Winkler foundation to elastic substrate

The response of an elastic substrate of Young's modulus E_s can be described through an *effective stiffness* $K^{\rm eff} = E_s/\ell$, where ℓ is the characteristic lateral scale of a surface deformation [45]. We start by assuming the existence of some $E_{s,\rm soft}$, such that for $E_s > E_{s,\rm soft}$ the system is in the low-deformability regime, and address later the actual dependence of $E_{s,\rm soft}$ on the parameters t, R, E_f.

In the low-deformability regime, where the deformation of the spherical substrate is only at the small wavelength and amplitude of the wrinkle pattern, the scale ℓ is the wrinkle wavelength, $\lambda \sim t(E_f/E_s)^{1/3}$, of a compressed film attached to compliant substrate [46]. The effective stiffness is thus $K^{\rm eff} = E_s/\lambda = t^{-1}(E_s^4/E_f)^{1/3}$, and the deformability parameter becomes $\tilde{K}^{\rm eff} = K^{\rm eff}R^2/(E_f t) = (E_s/E_f)^{4/3}/\tilde{t}^2$. Replacing $\tilde{K}$ with $\tilde{K}^{\rm eff}$ allows us to evaluate the energy $u^{\rm wr}$ of the wrinkled state by transforming the two parts of the energy [Eq. (50)]. The first part, $w_{\rm surf}$, which does not have an explicit dependence on the stiffness, is still given by Eq. (48). The second part is evaluated by replacing $K \to K^{\rm eff}$ in Eq. (49b), and we thus obtain $u^{\rm sub} \sim (E_s/E_f)^{2/3}\phi$.

In order to draw a schematic diagram analogous to Fig. 7(b), which describes the energetically favorable states in the low-deformability regime upon variation of ϕ and $\tilde{t}$, it is natural to consider some fixed, small values of the mechanical tension δ_m [similarly to Fig. 7(b)] and of the ratio E_s/E_f (which replaces $\tilde{K}$). Recalling that the energy of the axisymmetric state, which does not depend explicitly on the stiffness, is still given by Eq. (29), we draw in Fig. 8 three diagrams, which correspond to regimes II and regimes III-A and III-B, where the prolamination effect is predicted [47]. As Fig. 8 shows, regimes II, III-A, and III-B are distinguished by the value of the ratio E_s/E_f. Inspection of Fig. 8 allows us to characterize, similarly to Sec. V A, the response to increasing values of ϕ in the low-deformability regime.

(i) Regime II, at which the film is unwrinkled and delaminates from the substrate at $\phi = \phi_{\rm rig} = \sqrt{\delta_m}$ [Eq. (1)], corresponds to $(E_s/E_f)^{2/3} > \sqrt{\delta_m}$. In dimensional units, this leads us to identify regime II as

$$E_s > E_{s,\rm rig}; \quad \text{where} \quad E_{s,\rm rig} \sim \frac{\gamma^{3/4}E_f^{1/4}}{t^{3/4}}. \tag{57}$$

(ii) Regime III-A is defined by $\delta_m < (E_s/E_f)^{2/3} < \sqrt{\delta_m}$, which in dimensional units reads

$$\frac{\gamma^{3/2}}{E_f^{1/2}t^{3/2}} < E_s < E_{s,\rm rig}. \tag{58}$$

In this regime, the film becomes wrinkled at

$$\phi_{\rm wr} \sim (E_s/E_f)^{2/3}, \tag{59a}$$

and delamination occurs at

$$\phi_{\rm def} \sim \sqrt{\delta_m}(E_f/E_s)^{2/3} = \frac{\gamma^{1/2}E_f^{1/6}}{E_s^{2/3}t^{1/2}}. \tag{59b}$$

(iii) Regime III-B is defined by $(E_s/E_f)^{2/3} < \delta_m$ and $E_s > E_{s,\rm soft}$, which in dimensional units reads

$$E_{s,\rm soft} < E_s < \frac{\gamma^{3/2}}{E_f^{1/2}t^{3/2}}, \tag{60}$$

where $E_{s,\mathrm{soft}}$ is defined below. Note that our discussion of the analogous regime III-B in Sec. V A shows that the coverage fractions at which wrinkling and delamination occur do not depend explicitly on the stiffness parameter. Hence, as can be seen also from Fig. 8, we obtain expressions for ϕ_{wr} and ϕ_{def} which are identical to Eq. (56).

(iv) Regime I: Turning now to the high-deformability regime, we note that here the spherical substrate undergoes a significant deformation beneath the attached film, and hence the characteristic lateral scale for the deformation is the film's size W, rather than the wrinkle wavelength λ. Hence, the effective stiffness is $\tilde{K}^{\mathrm{eff}} \sim E_s/W$. Substituting this expression in Eq. (52), we obtain $E_{s,\mathrm{soft}} \sim E_f t W/R^2 = E_f \tilde{t}\sqrt{\phi}$. Thus, in contrast to a Winkler substrate, the tendency of a spherical compliant substrate to deform under the laminated film depends on the coverage fraction ϕ: The larger ϕ is, the larger should be E_s in order for the substrate to retain its shape under a laminated, axisymmetrically deformed (unwrinkled) film. This difference between Winkler's model and a compliant substrate underlies a small difference between Figs. 2(c) and 2(d): In Fig. 2(c), one may consider K_{soft} as a unique (ϕ-independent) value of the substrate stiffness below which the substrate deforms appreciably; in Fig. 2(d), the actual value of E_s below which the substrate undergoes significant deformation, does depend on ϕ.

Similarly to our discussion in Sec. V A, we want to find a value of $E_{s,\mathrm{soft}}$, which separates between the parameter regimes I, where the substrate deforms appreciably before the emergence of wrinkles, and regime III-B, where the formation of wrinkles enables lamination of the film without macroscopic deformation of the substrate. Hence, we substitute $\phi_{\mathrm{wr}} \sim \delta_m$ (which is the minimal value of ϕ for which the film is azimuthally compressed) in the expression $E_{s,\mathrm{soft}}(\phi) \sim E_f \tilde{t}\sqrt{\phi}$ and thus identify the high-deformability regime I as

$$E_s < E_{s,\mathrm{soft}}; \quad \text{where} \quad E_{s,\mathrm{soft}} \sim \frac{\gamma^{1/2} E_f^{1/2} t^{1/2}}{R}. \tag{61}$$

Similarly to our discussion of Winkler's substrate, we note that Figs. 8 and 2(b) depict distinct projections of the full phase diagram of the model onto 2D hyperplanes in the 4D parameter space. In Fig. 8, the free parameters are ϕ and $\tilde{t}^{-1}$ (whereas E_s/E_f and δ_m are assumed fixed values). In Fig. 2(b), the plane is spanned by the dimensionless parameters E_s/E_f and $\Gamma/E_f R$, which are both independent of the thickness t and the coverage fraction ϕ. Similarly to Fig. 2(a), the purpose of Fig. 2(b) is to describe the various scenarios that the system undergoes upon increasing ϕ, for various values of the substrate's Young's modulus and curvature, and the strength of adhesion.

VI. ASYMPTOTIC ISOMETRY

Beyond its relevance for our problem, the structure of the wrinkle energy, Eq. (50), reflects a surprising fact: It is possible to impose a doubly curved shape on a solid film in a way that becomes asymptotically isometric to the undeformed film (namely, where all components of the strain tensor are being eliminated [48]). In contrast to the common usage of isometries in studies of elastic sheets, which refers to the limit of small thickness, the asymptotic process underlying the wrinklogami pattern is double, involving both small thickness of the sheet (quantified through the bendability, $\epsilon^{-1} \gg 1$) and a small exerted tension (quantified by the confinement $\alpha \gg 1$). In this section, we expand on the meaning of the asymptotic isometry. We highlight the generic nature of Eq. (50) and discuss its relevance for other physical systems.

A. When are thin sheets said to be isometric to their undeformed state?

One may distinguish between three classes of loading conditions that can be exerted on a thin elastic sheet.

(A) When a sheet is subjected to *purely tensile loads*, the exerted work is transmitted primarily to an elastic energy stored in the stress field [Eq. (16)]. This applies not only at simple setups when a load induces a uniform tensile stress across the sheet (e.g., pulling with equal force on all boundaries), but also when the induced stress is nonhomogenous and some zones in the sheet are wrinkled due to compression. An example is the Lamé problem [21], where an annular sheet is subjected to distinct radial tensile loads at its inner and outer edges, and part of the sheet develops radial wrinkles that relax the induced azimuthal compression. In such a case, the exerted work is transmitted to the tensile components of the compression-free stress field, and the energetic cost of the wrinkles [analogous to our u^{sub}, Eq. (49)] is a negligible fraction of that work [29].

In problems of type (A), the main effect of the exerted loads is the deformation of the metric (i.e., inducing strain), but the shape of the sheet remains close to its original, unstressed, planar shape.

(B) When a sheet is confined in space, the exerted forces are *purely compressive* and their associated work is transmitted solely to bending the sheet and deforming an attached substrate or becoming partitioned between the energies associated with bending the sheet and straining the midplane in small "stress focusing" zones. The first scenario occurs under uniaxial compression, where the sheet becomes buckled or wrinkled (due to an attached substrate), retaining everywhere a developable shape. The second scenario occurs when a sheet is confined into a ring [11,12] or a small box [15], where the deformed shape is developable almost everywhere, except at narrow zones [the vertex of a developable cone (d cone) or along a "minimal ridge"] that contain strain. Similarly, when a sheet attached to a compliant substrate is subjected to biaxial compression, the deformed shape is developable almost everywhere [49,50].

In most problems of type (B), the exerted forces barely affect the metric, but may have a significant effect on the shape of the sheet, which departs appreciably from a planar one. In numerous cases, a solution may be found by searching for a developable (or piecewise developable) shape–an isometric transformation of the planar sheet to a shape that is compatible with the geometric constraints imposed on it [11,12,51,52]. The sheet thus gets arbitrarily close to this isometric shape in the asymptotic limit $t \to 0$.

(C) The problem we address in this work represents another class of systems, where the sheet is subjected simultaneously to a geometric constraint by the spherical shape of the substrate that is imposed on the sheet and to a tensile load at its boundary. Here, in contrast to the first two classes (A,B), both

the metric and the shape of the sheet are affected in a nontrivial manner. However, our analysis in Sec. IV C [Eqs. (39)–(41)] shows that the deformation of the metric (i.e., the strain) does not stem from the spherical shape itself, but rather from the mechanical strain $\delta_m = \gamma/Y$ exerted at the boundary. Hence, the sheet does approach a nontrivial isometry, where the shape is close to a spherical cap whose Gaussian curvature is nonzero, but, notably, the limit underlying this behavior is doubly asymptotic, being associated with small thickness of the sheet (quantified by the inverse bendability ϵ) and small exerted tensile load (quantified by the ratio $\delta_m/\delta_g = \alpha^{-1}$).

B. Asymptotic isometry equation

With the above classification of loading types, Eq. (50) can be viewed as a specific example of a generic form for the energy in class (C). Here, a sheet of size W is attached to a sphere of radius R and becomes nearly strainless in the singular, doubly asymptotic limit of small thickness ($\tilde{t} \sim t/W \to 0$) and weak tensile load ($\delta_m = \gamma/Y \to 0$). In this limit, the energy consists of two relevant terms. The first one is the work, which is linear in the tensile load ($\sim\delta_m$) and overrides the straining energy, which is quadratic in this parameter ($\sim\delta_m^2$). The second term is the energetic cost u^{sub} of bending the sheet and the deformation of a substrate. The work term is directly proportional to the tensile load and is independent on the sheet's thickness; the second term vanishes as some power of the sheet's thickness. Since the two energetic components are determined by independent parameters, the work is essentially "decoupled" from the elastic energy stored in the sheet. This type of energetic structure is strictly different from the analogous one in classes (A) and (B). In class (A), the exerted work is transmitted primarily to straining the sheet; in class (B), the work is transmitted to bending the sheet and deforming a substrate (if the shape is developable) or to the elastic energy stored in the stress-focusing zones of the sheet (in the case of a piecewise-developable shape).

The simplified nature of our problem in the low-deformability regime ($\tilde{K}^{-1} \ll 1$) is reflected in two intimately related facts. First, the wrinkles are superimposed on the original profile of the spherical substrate, and hence the work term, Eq. (48), can be expressed using the radius R of the undeformed substrate. Second, the optimal wrinkle pattern is determined by balancing the bending modulus B and the actual substrate's stiffness K. As a consequence, the energy component u^{sub}, Eq. (49b), may be viewed as a straightforward generalization of the energetic cost of wrinkles in a rectangular sheet attached to a substrate of stiffness K under uniaxial compression [45,46]. In order to understand the broad relevance of the asymptotic isometry equation, of which Eq. (50) is one example, it is useful to briefly consider some more complicated examples of systems in class (C).

(i) If the spherical substrate is sufficiently soft, such that the deformability parameter $\tilde{K}^{-1} \gg 1$ (regime I in our classification in Sec. V A), we expect not only the formation of wrinkles but also flattening of the substrate beneath the attached sheet. Such a behavior is demonstrated by a sheet floating on a liquid drop [8] (or even by an inflated mylar balloon [53]), where $\tilde{K} = 0$, and the curved shape is imposed by exerting a uniform Laplace pressure P, balanced by the surface tension γ of the drop of radius $R = 2\gamma/P$ that pulls at the boundary of the sheet. When γ and the bending modulus B are sufficiently small, we expect the wrinkled shape to approach an asymptotic isometry, similarly to our system. However, since the drop flattens beneath the sheet, the radius of curvature becomes $R_{\mathrm{eff}} \gg R$, and the radial profile $\zeta(r)$ on which the wrinkles are superimposed is significantly different from a spherical profile [8]. The energy may still be expressed in a similar manner to Eq. (50), but the actual computations of the work term (which is proportional to γ/Y) and the bending energy associated with wrinkles (which is proportional to some power of $\tilde{t}$) are more complicated [6].

(ii) Another example is the indentation of thin sheets that are placed on an adhesive substrate or floating on a liquid bath [54]. For a free-standing sheet, poking is an example of type (B) in the above classification, whereby the sheet attains a d-cone shape everywhere except at a small, stress-focusing vertex, whose size vanishes with the sheet's thickness [11,12]. Such a deformation is not possible if the sheet is required to remain floating on the liquid bath, and a nontrivial pattern of wrinkles emerges. Despite its complexity, such a wrinkle pattern may also become isometric to the undeformed sheet in the doubly asymptotic limit of weak tension (exerted by the liquid at the sheet's edge) and small thickness. The presence of multiple external forces (indentation, liquid gravity, and surface tension) complicates the computation of the work and the bending energy [55].

(iii) A third example is an elastic ribbon that is stretched and twisted around its main axis, where a plethora of patterns—wrinkles, creases, and loops—has been observed [56,57]. In a recent theoretical study, it was noted that under a given twist (i.e., a geometric constraint that imposes a helicoidal shape with nonzero Gaussian curvature), the ribbon approaches an isometry in the doubly asymptotic limit of vanishing tensile load and ribbon's thickness [58]. It was further argued that such an asymptotic isometry may be attained through wrinkles that cover the whole ribbon and are superimposed on a helicoidal shape, or through a "creased helicoid" shape, in which the stress is focused in narrow zones, whose size vanishes in this limit. The energy of each of those asymptotically isometric patterns consists of a work (done by the stretching force) and bending energy, similarly to Eq. (50).

All of the above examples exhibit a more complex, morphologically richer behavior than our system. In addition to wrinklogami patterns, other patterns have been observed. In example (i), a "wrinkle-to-crumple" transition has been found upon increasing the Laplace pressure in the drop, whereby the stress appears to be localized in structures that resemble ridges and d cones [8]. In example (ii), a somewhat different transition has been observed upon increasing the indentation depth [54], resembling a "wrinkle-to-fold" transition in uniaxial compression of rectangular floating sheets [59,60]. In example (iii), various instabilities of the wrinkle pattern, which are also characterized by stress-localizing ridges and loops, have been observed upon increasing the twist on the ribbon or decreasing the exerted tension [57].

In the next section we discuss the reason for the relative complexity of those systems in comparison to the simpler kind of asymptotic isometry that we studied here.

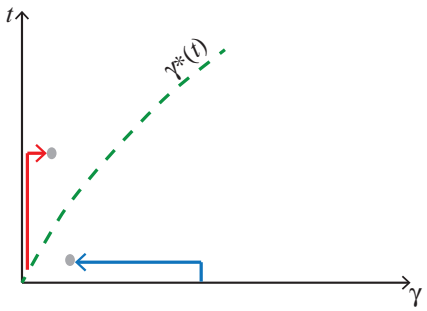

FIG. 9. (Color online) A schematic diagram that depicts the two distinct types of asymptotic isometries in problems of class (C), in which a film of thickness t is subjected to a fixed geometric constraint and a weak tensile load γ on its boundary. The horizontal and vertical axes are measures for the thickness and the exerted tensile load, respectively, for a given geometric constraint. (The actual, dimensionless measures are B/YW^2 and γ/Y). Below a curve $\gamma^*(t)$ we expect the emergence of a wrinklogami pattern, where the isometry is approached asymptotically by homogenous suppression of all stress components [blue (dark gray) trajectory: "route 2 to isometry" in our classification]. Above the curve $\gamma^*(t)$, we expect the shape to be approximated as a perturbation to real isometric transformation (i.e., developable or piecewise-developable map) of a 2D film, which often involves the formation of stress-focusing zones at ridges and vertices [red (gray) trajectory: "route 1 to isometry" in our classification].

C. Various routes for asymptotic isometry

In order to elucidate the various morphologies that are observed in problems of class (C), we present in this section a formal discussion, assuming a film subjected to some geometric constraint (e.g., twisting a ribbon by a given angle, indenting a film by a given amplitude, requiring a sheet to enclose a finite volume, etc.), characterized by bending modulus $B \sim E_f t^3$ and stretching modulus $Y \sim E_f t$, a characteristic lateral scale W (i.e., the radius of a circular film or the width of a ribbon), and a tension γ exerted on the film's boundary.

(i) *Route 1.* If it is possible to impose the geometric constraint without any tension (i.e., at $\gamma = 0$) then the shape can be described as a small perturbation of a perfectly isometric map of a 2D film, similarly to problems in class (B). The small parameter in this perturbative expansion, depicted schematically by the long leg of the red curve in Fig. 9, is $BW^2/Y \sim (t/W)^2$. The isometric shape, around which the expansion is carried out, may often consist of isolated curves or points with infinite curvature [11,12,61], which are regularized by this perturbative expansion, yielding stress-focusing zones [15]. Naturally, if the tension γ is nonzero, but is sufficiently small, the film's shape may still be described by this expansion, by adding to the energy the tensile work, as is depicted in the short leg of the red curve in Fig. 9. In a formal language, such a route to isometry is an expansion around the ordered limit: $\lim_{BW^2/Y\to 0}\lim_{\gamma/Y\to 0}$. As we described in Sec. VI B, an asymptotic isometry equation similar to Eq. (50) is valid also for such a state: The work term couples γ to the displacement field of the isometric map and overrides the straining energy (which is proportional to γ^2/Y); the energy u^{sub} for such a state stems from the bending cost of the isometric map at $\gamma = 0$ (e.g., formation of stress-focusing zones or a smoothly bent shape, such as for an unstretched, twisted ribbon).

(ii) *Route 2.* The above paragraph describes an expansion around an actual isometric shape of a 2D film (i.e., developable or piecewise-developable shape), in sharp contrast with the wrinklogami pattern, which we address in this paper. The first step in our derivation in Sec. IV, depicted by the short leg of the blue curve in Fig. 9, starts with the singular limit of a film with a *finite* modulus Y and $B = 0$, on which some tension $\gamma > 0$ is exerted. The compression-free stress is attained by such a "virtual" film through a wrinkling pattern with vanishing wavelength, and the energy u^{sub} is the energetic cost of wrinkles for a small $B > 0$. At the second step, depicted by the long leg of the blue curve, we assume the tension is reduced, such that the energy stored in the tensile component in the compression-free stress field may become arbitrarily small. In a formal language, this asymptotic route to isometry entails an expansion around the ordered limit, $\lim_{\gamma/Y\to 0}\lim_{BW^2/Y\to 0}$, which is strictly different from the one underlying route 1.

Thus, we recognize the existence of two distinct routes for isometric response of a thin film to a geometric constraint. Both routes lead to vanishing energetic cost in the singular limit of a vanishing film's thickness and exerted tensile load. The parameter regimes at which each of the two routes is valid are depicted by the green curve $\gamma^*(t)$ in Fig. 9: Route 1, where the film's shape may be approximated by an actual isometric, developable or piecewise-developable map of a 2D sheet, is valid at large ratios between the thickness and the tensile load (above the green curve). Route 2, where the film approaches isometry in a nondevelopable fashion, through a wrinklogami pattern with a smooth distribution of stress, cannot be approximated by any isometric shape of a 2D sheet and is valid at a small thickness/tension ratios (below the green curve).

We posit that the existence of two parameter regimes at the doubly asymptotic limit $(t \to 0, \gamma \to 0)$, at which strictly different types of deformations are expected, underlies phenomena such as "morphological phase transitions" in problems of class (C). Such a transition, which should become sharper as $t \to 0$, is expected in the vicinity of a curve $\gamma^*(t)$, depicted in Fig. 9. The universal aspect of such a transition, common to problems in class (C), is encapsulated in the asymptotic law: $\gamma^*(t) \to 0$ as $t \to 0$. The nonuniversal features of the transition, which may vary between systems, are in the exact function $\gamma^*(t)$ and, furthermore, in the actual shapes associated with the two routes to isometry. For the indentation of a floating sheet, such a morphological transition could be the observed wrinkle-to-fold transition [54]; for a floating film on a liquid drop, this mechanism may underlie a wrinkle-to-crumple transition [8]; for a stretched-twisted ribbon, such a scenario may explain some of the observed morphological transitions between various helicoidlike shapes [58]. In our system, such a morphological transition may not be dramatic, since the low deformability of the substrate forces the film to remain close to the substrate's spherical shape; hence, any observed difference between the two routes is likely to be minor.

VII. SUMMARY

Our main goal in this paper was to develop a theoretical framework for understanding the behavior of thin adhesive films on curved substrates. The elementary model we introduced here elucidates the dramatic difference between adhesion on rigid and deformable substrates and led us to predict the prolamination effect: An adhesive film may remain laminated on a curved, slightly deformable substrate, by developing a wrinkle pattern (wrinklogami) that does not affect the macro-scale shape of the substrate. A central feature, reverberated by Fig. 2, is the prevalence of the parameter regime III, at which the prolamination effect is expected, for very thin films. This prediction, which we expect to remain valid also for more complicated models of adhesion (e.g., inhomogeneous substrate with nonspherical shape), highlights the broad potential usage of the prolamination effect for technologies that employ ultrathin polymer films as well as crystalline sheets, most notably graphene.

Beyond its importance for adhesion phenomena, the wrinklogami pattern that we found here is an example of *asymptotic isometry*, whereby the film becomes strainless in the limit of small thickness and weak tensile load exerted on its edge. This asymptotic isometry concept, which characterizes thin sheets under sufficiently weak tensile loads, generalizes the standard usage of isometric maps, often used to describe the morphologies of elastic sheets under purely compressive loads. We proposed a general mechanism for morphological transitions between distinct types of asymptotic isometries, which may underlie various phenomena, such as wrinkle-to-fold transition in the indentation of floating films [54] and wrinkle-to-crumple transition in elastic sheets on liquid drops [8]. We hope to apply the asymptotic isometry equation, whose general structure we derived in this paper, to study the universal and nonuniversal features of such morphological transitions.

ACKNOWLEDGMENTS

We acknowledge support from UMass MRSEC on Polymers, NSF CAREER Award No. DMR-11-51780, and the hospitality of the Aspen center for physics, where part of the manuscript was written. We thank P. Buchak, G. Grason, R. Kohn, N. Menon, H.-M. Nguyen, C. Santangelo, and D. Vella for many discussions.

APPENDIX A: THE MENISCUS ENERGY

The energy associated with the local, Winkler-type restoring force is given in Sec. II B 3:

$$\bar{U}_{\rm Win} = \frac{K}{2}\int_0^{2\pi} d\theta \int_0^{W} r dr\, (\zeta - r^2/2R)^2 + \bar{U}_{\rm men}. \quad \text{(A1)}$$

Here we elaborate on the energetic contribution $\bar{U}_{\rm men}$. This term is associated with the "meniscus," at some zone $r > W$, across which the deformed substrate recovers its spherical shape,

$$\bar{U}_{\rm men} = \frac{K}{2}\int_{r>W} dx^2\, [r(\mathbf{x}) - R]^2, \quad \text{(A2)}$$

where the integral is over the surface of the substrate not covered by the film, and $r(\mathbf{x})$ is the distance of a point $\mathbf{x}$ on the substrate's surface from the center of the undeformed sphere. We may evaluate $\bar{U}_{\rm men}$ by noting that the substrate's surface recovers its spherical shape at a distance $\ell \approx \sqrt{\gamma/K}$ from the boundary $r = W$. This distance reflects an exponential decay of the meniscus shape, which stems from solving the equation $\gamma\ \delta\zeta'' - K\ \delta\zeta = 0$ for $r > W$ subjected to some boundary value $\delta\zeta_{(r=W)}$ and required to vanish $[\delta\zeta(r) \to 0]$ at $r \to \infty$. Here $\delta\zeta(r)$ is the deviation of the substrate's surface from its original, spherical shape $\zeta_{\rm sph}(r)$.

This approximation, valid for $W/R \ll 1$ and $\gamma/KR^2 \ll 1$ (see below), is identical to the meniscus of a flat liquid interface with surface tension γ and density $K = \rho g$, originating as a Euler-Lagrange equation of the approximated energy density $\frac{1}{2}[\gamma(\delta\zeta')^2 + K\delta\zeta^2]$ of the substrate surface that is not covered by the film. The energetic cost of the meniscus can be thus approximated as

$$\bar{U}_{\rm men} \approx \frac{1}{2}\sqrt{\gamma K}\,\delta\zeta(W)^2. \quad \text{(A3)}$$

Similarly to our derivation of Eq. (11), the meniscus energy $\bar{U}_{\rm men}$ gives rise to a *normal* boundary force $-\delta\bar{U}/\delta\zeta(W)$ exerted on the film at $r = W$:

$$F_n(W) = -\sqrt{\gamma K}\,\delta\zeta(W). \quad \text{(A4)}$$

We note, however, that in the parameter regime on which we focus our study (where $\tilde{K}, \alpha, \tilde{t}^{-1} \gg 1$), this force is negligible with respect to the tangential boundary force, Eq. (11), and therefore one can safely ignore the meniscus effect by assuming that the film approaches smoothly the substrate surface, namely,

$$\begin{aligned} \zeta(W) &= \zeta_{\rm sph}(W) \approx -W^2/2R, \\ \zeta'(W) &= \zeta'_{\rm sph}(W) \approx -W/R, \end{aligned} \quad \text{(A5)}$$

where we used, as usual, $W/R \ll 1$ to simplify the above equation.

In fact, the negligibility of the meniscus effect [and consequently the use of the BCs Eq. (A5)] may be valid also for a highly deformable substrate ($\tilde{K}^{-1} \gg 1$), as long as the meniscus zone is sufficiently smaller than the radius R of the spherical substrate. Using our dimensionless parameters, this implies that the BCs (A5) are valid as long as

$$\tilde{K} \gg \delta_m. \quad \text{(A6)}$$

Since the mechanical strain $\delta_m = \gamma/(E_f t) \ll 1$, we expect that the meniscus has a negligible effect even at the high-deformability regime (i.e., when the substrate deforms appreciably beneath the film), as long as $\tilde{K}$ exceeds δ_m. We will discuss elsewhere [6] the qualitative change in the system's behavior when $\tilde{K}$ becomes smaller than this minimal value, a situation which is particularly relevant for the problem of a sheet on a liquid drop (where $\tilde{K} = 0$).

APPENDIX B: THE SUBDOMINANT ENERGY $u^{\rm sub}$

In order to evaluate the wrinkle number m and its associated energy cost $u^{\rm sub}$, we follow [29,45] and consider the normal

force balance, Eq. (17a), substituting for $\zeta(r,\theta)$ the wrinkle shape, Eq. (32a). [Other oscillatory terms, such as $\sigma_{r\theta}\frac{d}{dr}\zeta_\theta \propto \sin(2m\theta)$, have negligible energetic contribution with respect to the primary oscillatory terms $\propto\cos(m\theta)$.] As a consequence of the divergence of the wrinkle number m in the singular limit $\epsilon \to 0$, we note that this equation could be simplified, to leading order in the amplitude f, as

$$B\frac{m^4}{r^4}f - \left(\sigma_{rr}^{(0)}\frac{d^2}{dr^2}f + \sigma_{rr}^{(m)}\frac{d^2}{dr^2}\zeta_{\rm sph}\right) + Kf = -\frac{m^2}{r^2}\sigma_{\theta\theta}f, \tag{B1}$$

where we used the superscript notations that were defined in Sec. IV C. The right-hand side is the destabilizing term (that derives from the energetic gain of compression release through out-of-plane buckling), and the left-hand side consists of the restoring forces (i.e., associated with energetic costs) that favor small wrinkle amplitude f. Note that the coupling of the radial stress to the radial component of the curvature yields two terms. The first term is associated with the coupling of the "pretension" $\sigma_{rr}^{(0)}$, Eq. (37), with the excess radial curvature $\frac{d^2}{dr^2}f$ along the wrinkle's direction [45]. The second term, $\sigma_{rr}^{(m)}\frac{d^2}{dr^2}\zeta_{\rm sph}$, stems from the coupling of the substrate's curvature ($\zeta_{\rm sph}^{''}$) to the oscillatory, wrinkle-induced perturbation to the radial stress: $\sigma_{rr}^{(m)} = -(E_f t)\frac{d^2}{dr^2}\zeta_{\rm sph} f$, which we evaluated with the aid of Eqs. (45), (3a), and (4a). We expand elsewhere on the generic nature of such a restoring force, which is induced by a curvature that is imposed on a film. The last restoring force, Kf, stems from the actual stiffness of the spherical substrate. The energetic costs associated with these restoring forces, are, respectively,

$$\frac{1}{4}\int_L^W rdr\ B\frac{m^4 f^2}{r^4} \sim \epsilon\phi^2 m^2, \tag{B2a}$$

$$\frac{1}{4}\int_L^W rdr\ \sigma_{rr}\left(\frac{d}{dr}f\right)^2 \sim \delta_m\phi\, m^{-2}, \tag{B2b}$$

$$\frac{1}{4}\int_L^W rdr\ (E_f t)\left(\frac{d}{dr}\zeta_{\rm sph}\right)^2 f^2 \sim \phi^2\, m^{-2}, \tag{B2c}$$

$$\frac{1}{4}\int_L^W rdr\ Kf^2 \Rightarrow u_{\rm subst} \sim \phi^2\tilde{K}\, m^{-2}, \tag{B2d}$$

where we used the slaving condition, Eq. (43) together with the approximation $u_r^{(0)} \approx -r^3/6R^2$ [which is valid in the large confinement regime, see Eq. (42)] to eliminate any explicit dependence on the wrinkle profile $f(r)$, and Eq. (37) for the radial tension σ_{rr}. The radial derivative $\frac{d}{dr}f$ is estimated as f/W, recalling that at large confinement the wrinkles prevail the whole film [see Eq. (38)], and hence the characteristic radial scale for the variation of the wrinkle profile $f(r)$ is W. An additional factor $1/2$ originates from the azimuthal integration of $\cos^2(m\theta)$, and all energies are normalized, per our convention, by $(E_f t)W^2$.

An inspection of the three energetic costs in Eqs. (B2b)–(B2d) reveals that all of them are proportional to m^{-2}, so we need to consider only the largest of them; the balance of this largest-among-three with the bending energy, Eq. (B2a), which is proportional to m^2, yields the energetically favorable wrinkle number [45]. Since we consider the low-deformability regime, $\tilde{K}^{-1} \ll 1$, and address the large confinement asymptotics $\alpha = \phi/\delta_m \to \infty$, the largest among the three terms (B2b)–(B2d) is the last one, which stems from the actual stiffness of the substrate. This type of energy balance is typical of "compressional wrinkles" that are formed under uniaxial compression of a thin film on compliant substrate [46]. We thus obtain the wrinkle number from the balance,

$$\tilde{K}\phi^2 m^{-2} \sim \epsilon\phi^2 m^2 \ \Rightarrow\ m \sim \left(\frac{\tilde{K}}{\epsilon}\right)^{1/4}, \tag{B3}$$

and the associated energy,

$$u^{\rm sub} \sim \sqrt{\tilde{K}\epsilon}\phi^2. \tag{B4}$$

For a given set of "pristine" parameters $\tilde{t}, \tilde{K}, \delta_m$, this energy is given as a function of ϕ by the expression

$$u^{\rm sub} \sim \tilde{t}\sqrt{\tilde{K}}\phi. \tag{B5}$$

[1] H. C. Ko *et al.*, Nature (London) **454**, 748 (2008).
[2] M. D. Fries and Y. K. Vohra, J. Phys. D: Appl. Phys. **35**, L105 (2002).
[3] C. Majidi and R. S. Fearing, Proc. R. Soc. London, Ser. A **464**, 1309 (2008).
[4] J. Hure, B. Roman, and J. Bico, Phys. Rev. Lett. **106**, 174301 (2011).
[5] J. Hure, B. Roman, and J. Bico, Phys. Rev. Lett. **109**, 054302 (2012).
[6] E. Hohlfeld *et al.* (unpublished).
[7] D. Vella *et al.*, Proc. Natl. Acad. Sci. USA **106**, 10901 (2009).
[8] H. King, R. D. Schroll, B. Davidovitch, and N. Menon, Proc. Natl. Acad. Sci. USA **109**, 9716 (2012).
[9] B. I. Yakobson, C. J. Brabec, and J. Bernholc, Phys. Rev. Lett. **76**, 2511 (1996).
[10] M. Yamamoto, O. Pierre-Louis, J. Huang, M. S. Fuhrer, T. L. Einstein, and W. G. Cullen, Phys. Rev. X **2**, 041018 (2012).
[11] M. Ben Amar and Y. Pomeau, Proc. R. Soc. London, Ser. A **453**, 729 (1997).
[12] E. Cerda and L. Mahadevan, Phys. Rev. Lett. **80**, 2358 (1998).
[13] B. A. DiDonna and T. A. Witten, Phys. Rev. Lett. **87**, 206105 (2001).
[14] A. V. Pogorelov, *Bending of surfaces and stability of shells* (American Mathematical Society, Providence, RI, 1988).
[15] T. A. Witten, Rev. Mod. Phys. **79**, 643 (2007).
[16] S. Deboeuf, E. Katzav, A. Boudaoud, D. Bonn, and M. Adda-Bedia, Phys. Rev. Lett. **110**, 104301 (2013).

[17] J. Shim, C. Perdigou, E. R. Chen, K. Bertoldi, and P. M. Reis, Proc. Natl. Acad. Sci. USA **109**, 5978 (2012).

[18] D. A. Huffman, IEEE Trans. Comput. **C-25**, 1010 (1976).

[19] M. A. Dias and C. S. Santangelo, Europhys. Lett. **100**, 54005 (2012).

[20] L. D. Landau and E. M. Lifshitz, *Theory of elasticity*, 3rd ed. (Butterworth-Heinemann, New York, 1986).

[21] S. P. Timoshenko and J. N. Goodier, *Theory of elasticity* (McGraw Hill, New York, 1970).

[22] E. H. Mansfield, *The bending and stretching of plates* (MacMillan, New York, 1964).

[23] Let us emphasize that Eq. (3) describes the geometric (strain-displacement) relation only for $|\nabla \mathrm{u}| \ll 1$ (which necessarily implies $|\varepsilon_{ij}| \ll 1$), while the Hookean (stress-strain) response only requires $|\varepsilon_{ij}| \ll 1$ [which may be satisfied even in a situation where the gradient $|\nabla \mathrm{u}|$ is not small and the geometric relation, Eq. (3), is not valid].

[24] The Winkler energy U_{Win} is appropriate for an elastic layer of thickness H and modulus E above a rigid foundation when the characteristic length scale for deformations of the film $\gg H$. For such a system, $K \sim E/H$.

[25] Equation (9b) was obtained from the axisymmetric map $\mathrm{u}_r(r) = -r^3/8R^2, \zeta(r) = \zeta_{\mathrm{sph}}(r) = -r^2/2R$ that projects the disk onto the (rigid) spherical substrate by preserving its area (where we assume $W/R \ll 1$): $\epsilon_{ii} = \partial_r \mathrm{u}_r + (\frac{d\zeta}{dr})^2/2 + \mathrm{u}_r/r = 0$. Note that this map is obtained in the limit $\tilde{K} \to \infty, \alpha \to \infty$ of the axisymmetric laminated state (see Sec. III).

[26] For the case of highly deformable substrate (i.e., sufficiently small K, or more precisely, $\tilde{K} \ll 1$, where $\tilde{K}^{-1}$ is the deformability parameter), the film may become laminated, even if $\Gamma > E_f t^3/R^2$, by flattening the substrate such that the curvature of the deformed substrate is $R_{\mathrm{eff}} \gg R$ and the bending energy is substantially reduced. Due to this effect, the lower bound $\Gamma/E_f R \sim (t/R)^3$ in our phase diagram is strictly valid only for sufficiently large K (corresponding to regimes II, III but not to regime I). The balance of bending energy and adhesion energy on a highly deformable substrate underlies the "capillary origami" phenomenon of a film on a liquid drop [35].

[27] The definition (21) of the deformability parameter seems to be different from Eq. (23) of [31]. However, the work reported in [31] addressed the "weak confinement" regime ($\alpha \gtrsim \alpha^*$), where $\gamma/W^2 \approx 8Y/R^2$, such that the two definitions are nearly identical. The definition given in the current paper is more suitable for the general case, yielding naturally the identification of the low-deformability parameter regime through $\tilde{K}^{-1} \gg 1$ [Eq. (31)].

[28] As we discussed above [after Eq. (11)], we assume for the simplicity of the discussion $\Gamma \approx \gamma$, where γ is the surface tension of the substrate. Our analysis is valid, up to a numerical pre-factor that does not affect the scaling behavior, for any finite ratio of γ/Γ.

[29] B. Davidovitch *et al.*, Proc. Natl. Acad. Sci. USA **108**, 18227 (2011).

[30] B. Davidovitch, R. D. Schroll, and E. Cerda, Phys. Rev. E **85**, 066115 (2012).

[31] G. M. Grason and B. Davidovitch, Proc. Natl. Acad. Sci. USA **110**, 12893 (2013).

[32] K. B. Toga, J. Huang, K. Cunningham, T. P. Russell, and N. Menon, Soft Matter **9**, 8289 (2013).

[33] M. Pineirua, N. Tanaka, B. Roman, and J. Bico, Soft Matter **9**, 10985 (2013).

[34] E. Hohlfeld, Ph.D. thesis, Harvard University, 2008.

[35] C. Py, P. Reverdy, L. Doppler, J. Bico, B. Roman, and C. N. Baroud, Phys. Rev. Lett. **98**, 156103 (2007).

[36] T. J. W. Wagner and D. Vella, Phys. Rev. Lett. **107**, 044301 (2011).

[37] We consider here the most elementary mechanism for wrinkling [a simply periodic shape, Eq. (32a)] and for delamination (such that the whole film detaches from the substrate). The actual instabilities may be more complex (e.g., wrinkling cascades, and a periodic pattern of blisters, respectively). Nevertheless, we do not expect this to affect the scaling laws that are presented in Fig. 2.

[38] M. Stein and J. M. Hedgepeth, NASA Technical Note D-813, National Aeronautics and Space Administration, Washington, DC, 1961.

[39] A. C. Pipkin, IMA J. Appl. Math. **36**, 85 (1986).

[40] D. J. Steigmann, Proc. R. Soc. London, Ser. A **429**, 141 (1990).

[41] The FT expansion is around the singular limit at which the sheet approaches the compression-free stress field, where the small parameter is the inverse bendability ϵ. Tension field theory may be considered as the leading order in this expansion. The FT expansion is strictly different from the standard postbuckling approach, valid in a narrow near-threshold (NT) parameter regime, which is essentially an expansion of FvK equations around the compressed, axisymmetric state, where the small parameter is the wrinkle amplitude (see [8,29,30]).

[42] The scaling $L/W \sim \alpha^{-1/3}$ is different from the result $L/W \sim \alpha^{-1/5}$ found for a wrinkled film on a liquid drop [8]. This reflects the difference between the soft liquid drop (akin to a highly deformable Winkler substrate with $\tilde{K}^{-1} \gg 1$) and the low-deformability case ($\tilde{K}^{-1} \ll 1$) addressed in the current study. A detailed discussion of this difference will appear elsewhere.

[43] Eq. (45) shows that $\mathrm{u}_r^{(m)}/f$ is finite, and therefore the oscillating component of the radial displacement $\mathrm{u}_r^{(m)} \to 0$ in the singular limit $\tilde{t} \to 0$ (similarly to f). Evaluation of the relevant contribution to the elastic energy [$\sim(\frac{d}{dr}\mathrm{u}_r^{(m)})^2$] shows that it is negligible compared to u^{sub}.

[44] P. Bella and R. V. Kohn, Commun. Pure Appl. Math. **67**, 693 (2014).

[45] E. Cerda and L. Mahadevan, Phys. Rev. Lett. **90**, 074302 (2003).

[46] N. Bowden *et al.*, Nature (London) **393**, 146 (1998).

[47] Since both parts of u^{wr} do not have explicit dependence on $\tilde{t}$, it is more transparent to draw in Fig. 8 three separate diagrams, rather than a single one, as in Fig. 7(b).

[48] We emphasize that there is no contradiction between this observation, which characterizes an asymptotic limit, and the well-known Gauss's theorema egregium, which implies that mapping of a planar surface to a doubly curved shape (i.e., with nonzero Gaussian curvature) cannot be purely isometric.

[49] B. Audoly and A. Boudaoud, J. Mech. Phys. Solids **56**, 2444 (2008).

[50] R. V. Kohn and H-M. Nguyen, J. Nonlin. Sci. **23**, 343 (2013).

[51] J. Dervaux and M. Ben Amar, Phys. Rev. Lett. **101**, 068101 (2008).

[52] Y. Klein, E. Efrati, and E. Sharon, Science **315**, 1116 (2007).

[53] G. I. Taylor, in *The scientific papers of Sir G.I. Taylor*, Vol. I, II, and III (Cambridge University Press, Cambridge, UK, 1958).
[54] D. P. Holmes and A. J. Crosby, Phys. Rev. Lett. **105**, 038303 (2010).
[55] D. Vella, J. Huang, N. Menon, T. P. Russell, and B. Davidovitch, Phys. Rev. Lett. **114**, 014301 (2015).
[56] A. E. Green, Proc. R. Soc. London, Ser. A **161**, 197 (1937).
[57] J. Chopin and A. Kudrolli, Phys. Rev. Lett. **111**, 174302 (2013).
[58] J. Chopin, V. Démery, and B. Davidovitch, J. Elasticity, doi:10.1007/s10659-014-9498-x.
[59] L. Pocivavsek *et al.*, Science **320**, 912 (2008).
[60] H. Diamant and T. A. Witten, Phys. Rev. Lett. **107**, 164302 (2011).
[61] A. P. Korte, E. L. Starostin, and G. H. M. van der Heijden, Proc. R. Soc. London, Ser. A **467**, 285 (2011).